ISSN 0234-5366

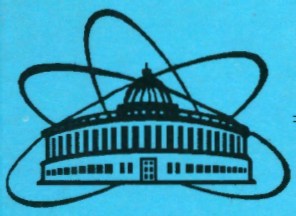

КРАТКИЕ СООБЩЕНИЯ ОИЯИ

JINR RAPID COMMUNICATIONS

4[96]-99

Издательский отдел ОИЯИ ДУБНА

JINR Publishing Department DUBNA

Объединенный институт ядерных исследований
Joint Institute for Nuclear Research

4[96]-99

КРАТКИЕ СООБЩЕНИЯ ОИЯИ

JINR RAPID COMMUNICATIONS

Дубна 1999

ОГЛАВЛЕНИЕ
CONTENTS

УДК 539.171.115

MEASUREMENTS OF THE TOTAL CROSS SECTION DIFFERENCE $\Delta\sigma_L(np)$ AT 1.59, 1.79, AND 2.20 GeV

V.I.Sharov[1], *S.A.Zaporozhets*[1], *B.P.Adiasevich*[2], *N.G.Anischenko*[1], *V.G.Antonenko*[2], *L.S.Azhgirey*[3], *V.D.Bartenev*[1], *N.A.Bazhanov*[4], *N.A.Blinov*[1], *N.S.Borisov*[3], *S.B.Borzakov*[5], *Yu.T.Borzunov*[1], *L.V.Budkin*[3], *V.F.Burinov*[3], *Yu.P.Bushuev*[1], *L.P.Chernenko*[5], *E.V.Chernykh*[1], *S.A. Dolgii*[1], *V.M.Drobin*[1], *G.Durand*,[6] *A.P.Dzyubak*[7], *A.N.Fedorov*[8], *V.V.Fimushkin*[1], *M.Finger*[3,9], *M.Finger,Jr.*[3], *L.B.Golovanov*[1], *G.M.Gurevich*[10], *A.Janata*[3,11], *A.V.Karpunin*[1], *B.A.Khachaturov*[3], *A.D.Kirillov*[1], *A.D.Kovalenko*[1], *A.I.Kovalev*[4], *V.G.Kolomiets*[3], *A.A.Kochetkov*[12], *E.S.Kuzmin*[3], *V.P.Ladygin*[1], *A.B.Lazarev*[3], *F.Lehar*[6], *A. de Lesquen*[6], *A.A.Lukhanin*[7], *P.K.Maniakov*[1], *V.N.Matafonov*[3], *A.B.Neganov*[3], *M.S.Nikitina*[12], *G.P.Nikolaevsky*[1], *A.A.Nomofilov*[1], *Tz.Panteleev*[5,13], *Yu.K.Pilipenko*[1], *I.L.Pisarev*[3], *N.M.Piskunov*[1], *Yu.A.Plis*[3], *Yu.P.Polunin*[2], *A.N.Prokofiev*[4], *P.A.Rukoyatkin*[1], *O.N.Shchevelev*[3], *V.A.Shchedrov*[4], *S.N.Shilov*[3], *Yu.A.Shishov*[1], *V.B.Shutov*[1], *M.Slunečka*[3,9], *V.Slunečková*[3], *A.Yu.Starikov*[1], *G.D.Stoletov*[3], *L.N.Strunov*[1], *A.L.Svetov*[1], *A.P.Tsvinev*[1], *Yu.A.Usov*[3], *V.I.Volkov*[1], *V.P.Yershov*[1], *A.A.Zhdanov*[4], *V.N.Zhmyrov*[3]

New results for the np spin-dependent total cross section difference $\Delta\sigma_L(np)$ at neutron beam kinetic energies of 1.59, 1.79, and 2.20 GeV are presented. Measurements of the $\Delta\sigma_L(np)$ energy dependence were carried out at the Synchrophasotron of the

[1]Laboratory of High Energies, JINR, 141980 Dubna, Moscow region, Russia.
[2]Scientific Centre "Kurchatov Institute", 123182 Moscow, Russia.
[3]Laboratory of Nuclear Problems, JINR, 141980 Dubna, Moscow region, Russia.
[4]Petersburg Nuclear Physics Institute, High Energy Physics Division, 188350 Gatchina, Russia.
[5]Frank Laboratory of Neutron Physics, JINR, 141980 Dubna, Moscow region, Russia.
[6]DAPNIA, CEA/Saclay, 91191 Gif-sur-Yvette Cedex, France.
[7]Kharkov Institute of Physics and Technology, 310108 Kharkov, Ukraine.
[8]Laboratory of Particle Physics, JINR, 141980 Dubna, Moscow region, Russia.
[9]Charles University, Faculty of Mathematics and Physics, V Holešovičkách 2, 18000 Praha 8, Czech Republic.
[10]Russian Academy of Sciences, Institute for Nuclear Research, 117312 Moscow, Russia.
[11]Academy of Sciences of the Czech Republic, Nuclear Research Institute, 25068 Řež, Czech Republic.
[12]Moscow State University, Faculty of Physics, 119899 Moscow, Russia.
[13]Bulgarian Academy of Sciences, Institute for Nuclear Research and Nuclear Energy, Tsarigradsko shaussee boulevard 72, 1784 Sofia, Bulgaria

Laboratory of High Energies of the Joint Institute for Nuclear Research in Dubna. A quasi-monochromatic neutron beam was produced by break-up of accelerated and extracted polarized deuterons. The neutrons were transmitted through a large proton polarized target. The values of $\Delta\sigma_L$ were measured as a difference between the np total cross sections for parallel and antiparallel beam and target polarizations, both oriented along the beam momentum. The results at the two higher energies were obtained using four combinations of two opposite polarization directions for both the beam and the target. Only one target polarization direction was available at 1.59 GeV. A fast decrease of $\Delta\sigma_L(np)$ with increasing energy above 1.1 GeV, as it was first seen from our previous data, was confirmed. The new results are also compared with model predictions and with the phase shift analysis fits. The $\Delta\sigma_L$ quantities for isosinglet state I=0, deduced from the measured values of $\Delta\sigma_L(np)$ and known $\Delta\sigma_L(pp)$ data, are given.

The investigation has been performed at the Laboratory of High Energies, JINR.

Измерения разности полных сечений $\Delta\sigma_L(np)$ при 1,59, 1,79 и 2,20 ГэВ

В.И.Шаров и др.

Представлены новые результаты по спин-зависимой разности полных np-сечений $\Delta\sigma_L(np)$ при кинетических энергиях пучка нейтронов 1,59, 1,79 и 2,20 ГэВ. Измерения энергетической зависимости $\Delta\sigma_L(np)$ выполнены на синхрофазотроне Лаборатории высоких энергий ОИЯИ. Квазимонохроматический пучок нейтронов создавался путем развала ускоренных и выведенных поляризованных дейтронов. Измерялось пропускание нейтронного пучка большой поляризованной протонной мишенью. Значения $\Delta\sigma_L$ определялись как разность полных np-сечений для параллельно и антипараллельно направленных поляризаций пучка и мишени, ориентированных вдоль направления импульса пучка. Результаты при двух высших энергиях были получены при использовании всех четырех комбинаций направлений поляризаций пучка и мишени. При энергии 1,59 ГэВ измерения выполнены только с одним направлением поляризации мишени. Подтверждено быстрое падение $\Delta\sigma_L(np)$ с ростом энергии выше 1,1 ГэВ, замеченное впервые по нашим предыдущим результатам. Новые данные сравниваются с предсказанием теоретических моделей и с последними решениями фазового анализа. Представлены также значения $\Delta\sigma_L$ для изосинглетного $I = 0$ np-состояния, полученные из измеренных величин $\Delta\sigma_L(np)$ и известных $\Delta\sigma_L(pp)$ данных.

Работа выполнена в Лаборатории высоких энергий ОИЯИ

Dedicated to the 275th anniversary of the Russian Academy of Sciences.

1. INTRODUCTION

This paper presents new results for the spin-dependent neutron-proton total cross section difference $\Delta\sigma_L(np)$ obtained in 1997 with a quasi-monochromatic polarized neutron beam and a polarized proton target (PPT). The values of $\Delta\sigma_L(np)$ were measured at neutron beam kinetic energies of 1.59, 1.79, and 2.20 GeV.

The free polarized neutron beam was produced by break-up of polarized deuterons accelerated and extracted at the Synchrophasotron of the Laboratory of High Energies (LHE) of the Joint Institute for Nuclear Research (JINR) in Dubna. This accelerator provides the highest energy polarized neutron beam, which can be reached now (3.7 GeV).

The spin-dependent observables $\Delta\sigma_L(np)$ and $\Delta\sigma_T(np)$ are defined as a difference in the np total cross sections for antiparallel and parallel beam and target polarizations, oriented longitudinally L and transverse T to the beam direction. Transmission measurements of the $\Delta\sigma_L(np)$ and $\Delta\sigma_T(np)$ energy dependences over 1.2–3.7 GeV have been proposed [1,2] and started [3,4,5] in Dubna. The main aim of this experimental program is to extend studies of the fundamental nucleon-nucleon (NN) interaction over a new highest energy region of free polarized neutron beams.

To implement the proposed $\Delta\sigma_{L,T}(np)$ experimental program, a large Argonne-Saclay polarized proton target (PPT) was reconstructed in Dubna [6,7], and a new polarized neutron beam line with suitable parameters was constructed and tested [8,9]. A set of necessary neutron detectors with corresponding electronics, an enough modern data acquisition system [10] and other needed equipment were also prepared, tuned and tested. Early in 1995, first three $\Delta\sigma_L(np)$ data points were successfully measured at neutron beam energies of 1.19, 2.49, and 3.65 GeV [3,4,5].

A new PPT polarizing solenoid [11] was constructed and tested at the JINR LHE for the purpose of continuing the $\Delta\sigma_{L,T}(np)$ measurements. In 1997, the presented values of $\Delta\sigma_L(np)$ were measured at 1.79 and 2.20 GeV using four combinations of two opposite polarization directions for both the beam and the target. Only one target polarization direction was available at 1.59 GeV. The preliminary results of this run were reported [12].

The NN total cross section differences $\Delta\sigma_L$ and $\Delta\sigma_T$ together with the spin-independent total cross section $\sigma_{0\mathrm{tot}}$ are linearly related to three nonvanishing imaginary parts of the NN forward scattering amplitudes via optical theorems. They are used for absolute normalization in any theoretical or phenomenological analysis. The $\Delta\sigma_{L,T}$ data check predictions of available dynamic models of strong interactions and provide an important contribution to a database of phase-shift analyses (PSA).

The observables $\sigma_{0\mathrm{tot}}$ in pp and np interactions have been measured in the last fifty years over a very large energy region. The np spin-dependent total cross section data are rare for lack of polarized neutron beams. All the observables are measured in pure inclusive transmission experiments.

The $\Delta\sigma_{L,T}(np)$ data at the same energy allow a direct determination of the imaginary parts of the spin dependent np forward scattering amplitudes. It is also possible to deduce the $\Delta\sigma_{L,T}$ nucleon-nucleon isosinglet ($I = 0$) parts using the measured np quantities and the existing pp (isotriplet $I = 1$) results.

The total cross section differences for pp scattering were first measured at the ANL-ZGS and then at TRIUMF, PSI, LAMPF, and SATURNE II. The results cover an energy range from 0.2 to 12 GeV. Other data points were measured at 200 GeV at FERMILAB for pp and $\bar{p}p$ interactions [13]. Measurements with incident charged particles need a different experimental set-up than neutron-proton experiments due to the contribution of electromagnetic interactions. The existing results are discussed in review [14] and references therein.

For the first time, the $\Delta\sigma_L(pn)$ results from 0.51 to 5.1 GeV were deduced from the $\Delta\sigma_L(pd)$ and $\Delta\sigma_L(pp)$ measurement at the ANL-ZGS in 1981 [15]. Taking a simple difference between the pd and pp results, corrected only for Coulomb-nuclear rescattering and

deuteron break-up, yields data in qualitative agreement with free np results. The correction for Glauber-type rescattering including 3-body state final interactions [16] provides a disagreement [14]. For these reasons, the ANL-ZGS pn results were omitted in the majority of existing PSA solutions.

The $\Delta\sigma_T$ and $\Delta\sigma_L$ results using free polarized neutrons, were first obtained at SATURNE II in 1987. These measurements yielded four points with relatively large errors [17]. These results have been completed by new accurate measurements at 9 to 10 energies, between 0.31 and 1.10 GeV for each observable [18,19]. The Saclay results were soon followed by PSI measurements [20] at 7 energy bins from 0.180 to 0.537 GeV using a continuous neutron energy spectrum. The PSI and Saclay sets allowed one to deduce the imaginary parts of np and $I = 0$ spin-dependent forward scattering amplitudes.[14,19].

The $\Delta\sigma_L(np)$ was also measured at five energies between 0.484 and 0.788 GeV at LAMPF [21]. A quasi-monoenergetic polarized neutron beam was produced in the $p + d \Rightarrow n + X$ scattering of longitudinally polarized protons. Large neutron counter hodoscopes had to be used because of a small neutron beam intensity.

At low energies, the $\Delta\sigma_L(np)$ at 66 MeV was measured at the PSI injector [22] and at 16.2 MeV in Prague [23]. The $\Delta\sigma_T(np)$ was determined at 9 energies between 3.65 and 11.6 MeV [24] in TUNL and at 16.2 MeV in Prague [25]. Recently in TUNL, the $\Delta\sigma_L(np)$ was measured at 6 energies between 4.98 and 19.7 MeV and $\Delta\sigma_T(np)$ at 3 other energies between 10.7 and 17.1 MeV. The latter results are still unpublished, and we refer to the George Washington University and Virginia Polytechnic Institute (GW/VPI) PSA database [26] (SAID SP99).

All JINR results are smoothly connected with the existing $\Delta\sigma_L(np)$ data at lower energies and show a fast decrease to zero between 1.1 and 2.0 GeV. They are compared with model predictions and the PSA fits. The values of the $I = 0$ part of $\Delta\sigma_L$ are also presented. The $\Delta\sigma_L(I = 0)$ and $\Delta\sigma_L(I = 1)$ energy dependences and hence a behaviour of spin dependent NN-amplitudes, are different over the measured energy range.

We give a brief determination of the measured observables in Section 2. Section 3 describes the method of the measurement. Essential details concerning the beams, the polarimeters, the experimental set-up and PPT are treated in Section 4. The data acquisition and analysis are described in Section 5. The results and discussion are presented in Section 6.

2. DETERMINATION OF OBSERVABLES

In this paper, we use the NN formalism and the notations for elastic nucleon-nucleon scattering observables from [27].

The general expression of the total cross section for a polarized nucleon beam transmitted through a PPT, with arbitrary directions of beam and target polarizations, $\vec{P}_B$ and $\vec{P}_T$, respectively, was first deduced in Refs. 28,29. Taking into account fundamental conservation laws, it is written in the form :

$$\sigma_{\rm tot} = \sigma_{0\rm tot} + \sigma_{1\rm tot}(\vec{P}_B, \vec{P}_T) + \sigma_{2\rm tot}(\vec{P}_B, \vec{k})(\vec{P}_T, \vec{k}), \qquad (2.1)$$

where $\vec{k}$ is a unit vector in the beam momentum direction. The term $\sigma_{0\rm tot}$ is the total cross section for unpolarized particles, and the $\sigma_{1\rm tot}$, $\sigma_{2\rm tot}$ are the spin-dependent contributions.

They are related to the measurable observables $\Delta\sigma_T$ and $\Delta\sigma_L$ by :

$$-\Delta\sigma_T = 2\sigma_{1\mathrm{tot}}, \tag{2.2}$$

$$-\Delta\sigma_L = 2(\sigma_{1\mathrm{tot}} + \sigma_{2\mathrm{tot}}), \tag{2.3}$$

called "total cross section differences". The negative signs for the $\Delta\sigma_T$ and $\Delta\sigma_L$ in Eqs.(2.2) and (2.3) correspond to a usual, although unjustified, convention in the literature. The $-\Delta\sigma_T$ and $-\Delta\sigma_L$ are measured as the differences of total nucleon-nucleon cross sections for parallel and antiparallel beam and target polarization directions. Polarization vectors are transversely oriented with respect to $\vec{k}$ for $-\Delta\sigma_T$ measurements and longitudinally oriented for $-\Delta\sigma_L$ experiments.

The total cross section differences are determined by an arbitrary pair of one parallel and one antiparallel beam and target polarization directions. For $\vec{P}_B$ and $\vec{P}_T$, both oriented along $\vec{k}$, we obtain four total cross sections :

$$\sigma(\rightrightarrows) = \sigma_{0\mathrm{tot}} + |P_B^+ P_T^+|\ (\sigma_{1\mathrm{tot}} + \sigma_{2\mathrm{tot}}), \tag{2.4a}$$

$$\sigma(\leftrightarrows) = \sigma_{0\mathrm{tot}} - |P_B^- P_T^+|\ (\sigma_{1\mathrm{tot}} + \sigma_{2\mathrm{tot}}), \tag{2.4b}$$

$$\sigma(\rightleftarrows) = \sigma_{0\mathrm{tot}} - |P_B^+ P_T^-|\ (\sigma_{1\mathrm{tot}} + \sigma_{2\mathrm{tot}}), \tag{2.4c}$$

$$\sigma(\leftleftarrows) = \sigma_{0\mathrm{tot}} + |P_B^- P_T^-|\ (\sigma_{1\mathrm{tot}} + \sigma_{2\mathrm{tot}}). \tag{2.4d}$$

In principle, an arbitrary pair of one parallel and one antiparallel beam and target polarization direction determines $\Delta\sigma_L$. Using two independent pairs, we also remove an instrumental asymmetry.

Bellow, we consider the neutron beam and the proton target. Since the $\vec{P}_B$ direction at the Synchrophasotron could be reversed every cycle of the accelerator, it is preferable to calculate $\Delta\sigma_L$ from measurements for $|P_B^+|$ and $|P_B^-|$ pairs with the same $\vec{P}_T$ orientation. The values of $|P_T^+|$ and $|P_T^-|$ are considered to be well-known as functions of time. Taking the difference of the total cross sections for the pair of $|P_B^+|$ and $|P_B^-|$, the spin-independent term drops out, and one can obtain:

$$-\Delta\sigma_L(P_T^+) = 2\ (\sigma_{1\mathrm{tot}} + \sigma_{2\mathrm{tot}})^+ = \frac{2\ [\sigma(\rightrightarrows) - \sigma(\leftrightarrows)]}{(|P_B^+| + |P_B^-|)\ |P_T^+|}, \tag{2.5a}$$

$$-\Delta\sigma_L(P_T^-) = 2(\sigma_{1\mathrm{tot}} + \sigma_{2\mathrm{tot}})^- = \frac{2\ [\sigma(\leftleftarrows) - \sigma(\rightleftarrows)]}{(|P_B^+| + |P_B^-|)\ |P_T^-|}. \tag{2.5b}$$

A left-right asymmetry, proportional to the mean value of the beam polarization

$$|P_B| = \frac{1}{2}(|P_B^+| + |P_B^-|) \tag{2.6}$$

is continuously monitored by a beam polarimeter.

The instrumental asymmetry cancels out giving the final results as a simple average

$$-\Delta\sigma_L = \frac{1}{2}[(-\Delta\sigma_L(P_T^+)) + (-\Delta\sigma_L(P_T^-))]. \tag{2.7}$$

This is discussed in detail in Section 4. The $\sigma_{0\,\mathrm{tot}}$, $\Delta\sigma_T$, and $\Delta\sigma_L$ are linearly related to the imaginary parts of the three independent forward scattering invariant amplitudes $a+b$, c and d via optical theorems :

$$\sigma_{0\,\mathrm{tot}} = (2\pi/K)\ \Im m\ [a(0)+b(0)], \tag{2.8}$$

$$-\Delta\sigma_T = (4\pi/K)\ \Im m\ [c(0)+d(0)], \tag{2.9}$$

$$-\Delta\sigma_L = (4\pi/K)\ \Im m\ [c(0)-d(0)], \tag{2.10}$$

where K is the CM momentum of the incident nucleon. Relations (2.9) and (2.10) allow one to extract the imaginary parts of the spin-dependent invariant amplitudes c(0) and d(0) at an angle of $\theta = 0^c$ from the measured values of $\Delta\sigma_L$ and $\Delta\sigma_T$. Note that the optical theorems provide the absolute amplitudes. These amplitudes are also determined by the PSA at any scattering angle. Using a direct reconstruction of the scattering amplitudes (DRSA), the absolute amplitudes are determined at $\theta = 0°$ only, whereas one common phase remains undetermined at any other angle. The PSA and DRSA approaches are complementary phenomenological analyses, as discussed in [30,31].

Using the measured values of $\Delta\sigma(np)$ and the existing $\Delta\sigma(pp)$ data at the same energy, one can deduce $\Delta\sigma_{L,T}(I=0)$ as :

$$\Delta\sigma_{L,T}(I=0) = 2\Delta\sigma_{L,T}(np) - \Delta\sigma_{L,T}(pp). \tag{2.11}$$

3. METHOD OF MEASUREMENT

If N_{in} is the number of neutrons entering the target and N_{out} the number of neutrons transmitted by the target into solid angle Ω subtended by a transmission detector from the center of the target, then the total cross section $\sigma(\Omega)$ is related to the measured quantities:

$$N_{\mathrm{out}} = N_{\mathrm{in}} \exp[-\sigma(\Omega) n x], \tag{3.1}$$

where n is the number of target atoms per cm^3, x is the target thickness (cm) and $N_{\mathrm{out}}/N_{\mathrm{in}}$ is the transmission ratio. The extrapolation of $\sigma(\Omega)$ towards $\Omega = 0$ gives the unpolarized total cross section σ_{tot}.

The number of polarizable hydrogen atoms n_H is only important in the $\Delta\sigma_{L,T}(\Omega)$ measurements. The $\Delta\sigma_{L,T}(\Omega)$ depends also on the polarizations $P_B^{\pm}$ and $P_T^{\pm}$ as shown in Eqs.(2.5). Summing over the events taken with one fixed target polarization P_T^+ or P_T^- and using Eqs.(2.5a) or (2.5b), we can obtain a double transmission ratio corresponding to a difference of two values of $\sigma(\Omega)$ for P_B^- and P_B^+

$$R^{\pm} = \frac{(N_{\mathrm{out}}/N_{\mathrm{in}})^-}{(N_{\mathrm{out}}/N_{\mathrm{in}})^+} = \exp\ [\Delta\sigma(\Omega)\ P_B P_T^{\pm} n_H x] \tag{3.2}$$

with the average P_B from Eq.(2.6). Since the measured monitor counts M are proportional to primary neutron flux N_{in} entering the PPT and the counts of the transmission detectors T are proportional to transmitted neutron intensity N_{out}, the neutron detector efficiencies drop down in Eq.(3.2). To determine the $\Delta\sigma_{L,T}(\Omega)$, we have

$$\Delta\sigma_L(\Omega, P_T^{\pm}) = \frac{1}{P_B . P_T^{\pm} . n_H . x} ln R(P_T^{\pm}). \tag{3.3}$$

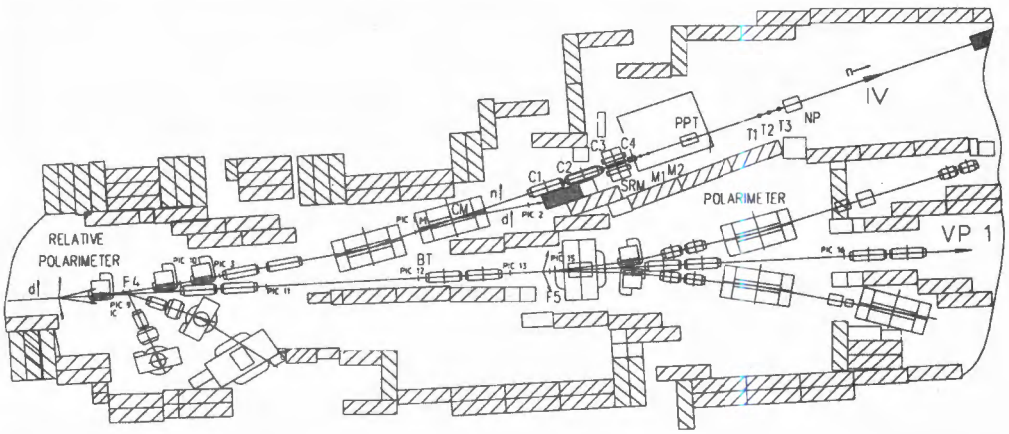

Fig. 1. Experimental set-up for the $\Delta\sigma_{L,T}(np)$ measurements. Layout of the set-up in the Experimental Hall. VP1 - beam line of extracted, polarized deuterons; 1V - beam line of polarized neutrons; BT - neutron production target; IC - ionization chamber for monitoring of deuteron beam intensity; PIC 1-3, 9-16 - multiwire proportional/ionization chambers for measurements of the deuteron beam profiles; CM - sweeping magnet; C1-C4 - set of neutron beam collimators; SRM - neutron spin rotating dipole; PPT - polarized proton target; and NP - neutron beam profilometer

We can neglect the extrapolation of $\Delta\sigma_L(\Omega)$ towards a zero solid angle ($\Omega \to 0$) due to the chosen sizes of the transmission detectors and their distances from the PPT [3,4,5]. The Saclay-Geneva (SG) PSA [31] at 1.1 GeV shows that the resulting value of $\Delta\sigma_L$ decreases at most by 0.04 mb for the angles covered by our detectors. This possible error seems to decrease with increasing energy as the PSA calculations at 1.0 GeV have shown.

The ratio of n_H to other target nuclei depends on the target material. The presence of carbon in the PPT beads adds the terms $\sigma_{\rm tot}(C)$ in Eqs.(2.4). These terms are spin-independent, and their contribution drops out in differences (2.5). The same occurs for ^{16}O and ^4He in the target. However, there are small contributions from ^{13}C and ^3He, which may be slightly polarized. This contribution was estimated to be $\pm$ 0.3 %. Uncertainties in the determination of P_B, P_T and $n_H.x$ are discussed in Section 4.

4. EXPERIMENTAL SET-UP

The experimental set-up (see Figs.1,2) for the $\Delta\sigma_{L,T}(np)$ measurements is described in [3,4,5]. We mention here only essential items important for the data analysis and results, as well as modifications and improvements of the apparatus and experimental conditions.

Both polarized deuteron and polarized free neutron beam lines [8,9], the two polarimeters [32,33], the neutron production target BT, collimators C1-C4, the spin rotation magnet SRM, the polarized proton target PPT [6,7,34], neutron beam monitors M1, M2, transmission detectors T1-T3 and the apparatus for monitoring the neutron beam profiles NP are shown in Figs.1,2. The associated electronics and the data acquisition system are also described in [3,4,5,10].

Deuterons were extracted at energies of 3.20, 3.60, and 4.40 GeV for the $\Delta\sigma_L(np)$ measurements, as well as at 1.60 GeV for the polarimetry purposes. The beam momenta p_d

were known with a relative accuracy of $\sim \pm 1$ %. The intensity of the primary polarized deuteron beam increased by a factor of ~ 3 to 4 with respect to the 1995 run. The average deuteron intensity over the run was $\sim 2 \times 10^9$ d/cycle. It was continuously monitored using two calibrated ionization chambers placed in the focal points F3 and F4 of the deuteron beam line before the neutron production target BT. In the 1997 run, different characteristics of the accelerated and extracted deuteron beam and the status of the used beam lines were in part available on the Laboratory Ethernet (cycle by cycle).

The beam of free quasi-monochromatic polarized neutrons was obtained by break-up of vector polarized deuterons at 0° in the BT. Neglecting the BT thickness, the laboratory momentum of neutrons $p_n = p_d/2$ with a momentum spread of FWHM $\simeq 5\%$ [35]. The BT contained 20 cm Be with a cross section of 8×8 cm^2. The passage of deuterons through air, windows and production target matter provided a deuteron beam energy decrease by 20 MeV in the BT centre, and the mean neutron energy decreased by 10 MeV [4]. The energies and laboratory momenta in the BT centre are quoted for the $\Delta\sigma_L$ results and the extracted beam energies are used for the beam polarization measurements.

The dimensions and positions of iron and brass collimators C1-C4 (Fig. 1) were the same as those described in [3,4,5]. An accurate measurement of the collimated neutron beam profiles was made in a dedicated run using nuclear photoemulsions. During the data acquisition, the position and X-,Y-profiles of the neutron beam were continuously monitored by a neutron profilometer NP with multiwire proportional chambers closely placed downstream the last transmission detector (see Figs.1,2).

The value and direction of proton beam polarization $\vec{P}_B(p)$ after deuteron break-up at 0° and for $p_p = p_d/2$ are the same as the vector polarization $\vec{P}_B(d)$ of the incident deuteron beam [36,37]. Assuming identical break-up conditions for neutrons, we have $\vec{P}_B(n) \simeq \vec{P}_B(p) \simeq \vec{P}_B(d)$. Then, one can measure $P_B(d)$ in order to know $P_B(n)$. During the run, the polarization $P_B(d)$ and hence the neutron beam polarization $P_B(n)$ were reversed every cycle, as requested.

The prepared neutron beam has the same vertical orientation of $P_B(n)$ as the accelerated and extracted deuteron beam. Such a neutron beam is suitable for the $\Delta\sigma_T(np)$ measurements. For the purpose of the $\Delta\sigma_L(np)$ measurements, we have to turn the neutron spins from the vertical to the longitudinal direction. This was done by the spin-rotating magnet SRM in the neutron beam line (Figs.1,2). The SRM magnetic field was continuously monitored by a Hall probe. The SRM setting and inhomogeneity of the magnetic field integral within the neutron beam tube can provide an additional systematic error of ± 0.2 %.

The measurement of $P_B(d)$ was carried out by the four-arm beam line polarimeter [32]. It consists of a liquid hydrogen target, situated at focus F5 of the extracted beam line VP1 (Fig.1), and two pairs of detector arms with recoil proton detection and magnetic analysis of scattered deuterons. The polarimeter can use a high intensity of deuterons. It determined the elastic dp scattering asymmetries at the kinetic energy of incident deuterons $T_{\rm kin}(d) =$ 1.60 GeV and at a square of the 4-momentum transfer $t = -0.15(\mathrm{GeV}/c)^2$. At this value of $T_{\rm kin}(d)$, the analyzing powers of this reaction are well known [38], and the chosen t-value is close to the maximum values of the analyzing powers. In principle, the $P_B(d)$ needs to be determined at one energy only since no depolarizing resonance exists [32]. On the other hand, the measurement requires to change the deuteron energy and to extract the beam in another beam line, what is a time-consuming operation. This polarimeter was used only

once before data acquisition and gave an average $|P_B(d)|$ of 0.524 ± 0.010 for positive and negative signs of the vector polarization . The possible systematic error of this measurement was ± 0.010. The admixture of the tensor components of the deuteron beam polarization, measured simultaneously by this polarimeter, was negligible.

The value of $P_B(p)$ was continuously monitored by another four-arm beam polarimeter [33] with a small acceptance of 7.1×10^{-4} sr during the data acquisition. The deuteron beam, considered as a beam of quasi-free protons and neutrons, collided with a CH_2 target, and quasi-free protons, scattered at 14° lab., were detected in coincidence with the protons detected by recoil arms. This polarimeter measured the *pp* left-right asymmetry on hydrogen and carbon at $T_{\rm kin}(p) = T_{\rm kin}(d)/2 = 0.80$ GeV. A simultaneous measurement together with the *dp* polarimeter gave the asymmetry $\epsilon(CH_2) = 0.2572 \pm 0.0071$. Subtracting the carbon and inelastic contributions, we obtained the following *pp* asymmetry on hydrogen $\epsilon(pp) = 0.2661 \pm 0.0073$.

The *pp* analyzing power A_{oono} was taken from the energy fixed GW/VPI-PSA [26] (SP99, solution 0.800 GeV) as well as from the SG-PSA [31] (solution 0.795 GeV). The values of $A_{oono}(pp)$ at 0.80 GeV were 0.4872 ± 0.0034 for the GW/VPI-PSA and 0.4821 ± 0.0009 for the SG-PSA. A mean value of 0.4846 ± 0.0017 provided $P_B(p) = P_B(d) = 0.549 \pm 0.015$.

The weighted average of both independent results from the two polarimeters, used for the calculations of the present results, was $|P_B(d)| = 0.532 \pm 0.008$. This is in excellent agreement with the value of $|P_B(d)| = |P_B(n)| = 0.533 \pm 0.009$ measured previously with the *dp* polarimeter at $T_{\rm kin}(d) = 1.662$ GeV and used in [3,4,5].

In 1995, the *pp* polarimeter provided only $\epsilon(CH_2) = 0.246 \pm 0.016$ at 0.831 GeV. If we apply the present ratio of $\epsilon(pp)/\epsilon(CH_2) = 1.0346$, we have $\epsilon(pp) = 0.255 \pm 0.017$. The discrete energy $A_{oono}(pp)$ predictions from the GW/VPI-PSA [26] (solution 0.850 GeV) and from the SG-PSA [31] (solution 0.834 GeV) give the mean value of 0.4824 ± 0.0048. We obtain $P_B(p) = P_B(d) = 0.528 \pm 0.035$ again in agreement with the *dp* polarimeter measurement.

Note that we have used the discrete energy PSA for the *pp* analyzing power calculations. Both PSA are locally energy-dependent and describe the measured observables at their own energies. The energy dependent PSA is not an adequate tool for the polarimetry purpose since the A_{oono} fit at a given energy may be smeared by all other fitted observables over a wide energy range.

We observed that $|P_b(d)|$ decreased for the running time tm (hours) as

$$P_d(tm) = P_d(tm = 0)\ (1 - 0.00154 \cdot tm)\ . \qquad (4.1)$$

The error of the linear term is $\pm$ 0.00013. Due to an unknown effect in the ion source, this decrease was independent of beam energy and was taken into account for the results. The global relative systematic error of $|P_b(d)|$ from all sources was estimated as ± 1.7 %.

The frozen-spin polarized proton target, reconstructed to a movable device [6,7,11,34], was used. The target material was 1,2-propanediol ($C_3H_8O_2$) with a paramagnetic Cr^V impurity having a spin concentration of 1.5×10^{20} cm^{-3} [39]. The propanediol beads were loaded into the thin wall teflon container 200 mm long and 30 mm in diameter placed inside the dilution refrigerator.

The weight of the propanediol beads for the completely filled container is 94.88 g. A uniform neutron intensity distribution over the target diameter is due to the collimator sizes. The target container, covering the neutron beam, was aligned along the beam axis.

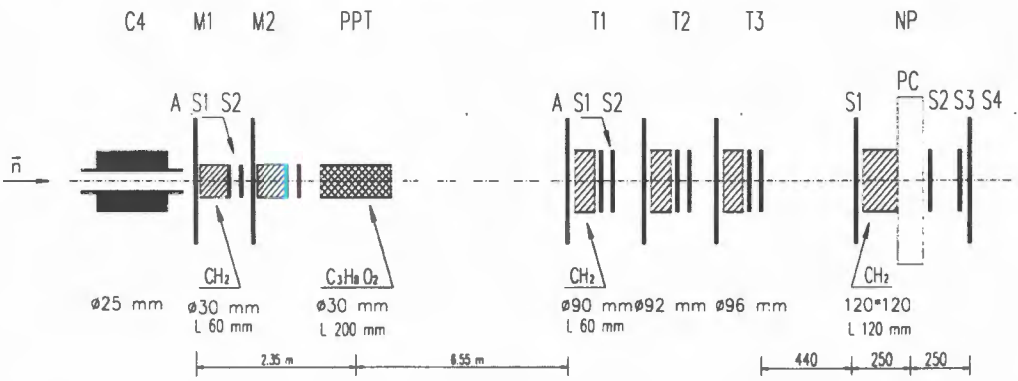

Fig. 2. Experimental set-up for the $\Delta\sigma_{L,T}(np)$ measurements. Layout of the detectors for the neutron transmission measurement. M1, M2 - monitor neutron detector modules; T1-T3 - neutron transmission detector modules; CH_2 - converters; A,S1-S4 - scintillation counters; PC - multiwire proportional chambers X,Y

In this experiment, the target was incompletely filled, and the measured weight of the beads was (73.25 $+0.80, -0.20$) g. This represents a ratio Q of 0.772 which decreases the number of hydrogen atoms per cm^2 for the target container completely filled in diameter over thickness $x' = Q \cdot x$. We have $n_H \cdot x = 8.878 \times 10^{23}/\text{cm}^2$ for full target filling and $Q \cdot n_H \cdot x = n_H \cdot x' = 6.854 \times 10^{23}/\text{cm}^2$ for the target filled over thickness x'. An additional effect on the number of hydrogen atoms per cm^2 is provided by a configuration of the beads in the target container. For the same weight of the beads, the effective number of hydrogen atoms per cm^2 is mimimal for incomplete filling with the horizontal plane of the beads. This kind of filling occured in our experiment. In this case, we have an effective value of the number of hydrogen atoms per cm^2

$$(n_H \cdot x)_{\text{eff}} = Q \cdot f \cdot n_H \cdot x = (6.405 \pm 0.19)\ 10^{23}/\text{cm}^2,$$

where the factor f includes all corrections for the configuration of propanediol beads inside the target container. The error contains uncertainties of all contributions.

The P_T measurements were carried out using a computer-controlled NMR system. The values of negative proton polarization were -0.772 at the beginning of data taking and -0.701 at the end (after 64 hours). The positive values of P_T were 0.728 and 0.710 after 34 hours, respectively. This corresponds to relaxation times of 1358 hours for P_T^+ and 663 hours for P_T^-. The relative uncertainty of the measured P_T values was estimated to be ± 5 %. This error includes uniformity measurements using the NMR data from three coils.

Neutron detector location and the associated electronics are described in [3,4,5]. The detector configuration is shown in Fig.2. The two neutron intensity monitors are denoted by M1 and M2, the three transmission detectors by T1, T2 and T3. Each detector M or T consists of a veto counter, a CH_2 radiator for a neutron produced charge-exchange reaction and two counters in coincidence. A stable power supply system was used for the photomultipliers.

The result of $\Delta\sigma_{L,T}$ is independent of neutron beam intensity if the probability of quasi-simultaneous detection of two neutrons in one transmission detector can be neglected. For

this reason, the efficiency of each detector must be relatively small, and each of the detectors must be independent of one another [4].

Dedicated tests were performed during an additional run with a high intensity unpolarized deuteron beam. Using the same transmission set-up, the neutron-carbon total cross section $\sigma_{\text{tot}}(nC)$ was determined at $T_{\text{kin}}(n) = 1.5$ GeV. For this purpose, a number of carbon targets of different thicknesses were inserted in the neutron beam line instead of the PPT. The measured value of $\sigma_{\text{tot}}(nC)$ agrees with the data from compilation [40].

5. DATA ANALYSIS

The following main information was recorded and displayed by the data acquisition system for each accelerator cycle:

labels of the beam polarization signs,

rates of the two calibrated ionization chambers used as primary deuteron beam intensity monitors,

rates of two neutron detectors M1 and M2 used as intensity monitors of the neutron beam incident on the PPT,

rates of three neutron transmission detectors T1, T2, and T3,

rates of the accidental coincidences for all neutron detectors M1, M2, T1, T2, T3,

rates of the left and right arms of the *pp* beam polarimeter.

Statistics at 2.2 and 1.8 GeV with P_T^- were recorded at the beginning of the run. Then, the data were taken at 2.20, 1.79 GeV, and 1.59 GeV with P_T^+. The results with P_T^- could not be obtained for the last energy.

The recorded data were then analysed in two steps. "Bad" files, as well as "empty" cycles and cycles with incorrect labels of the P_B signs, were removed in the first step. The number of "bad" cycles for the cumulated statistics represented a few tenths of a percent. The total statistics over the run obtained after the first step of the data analysis are shown in Table 1.

Since the statistics listed in one row were taken simultaneously, we see their monotonous decrease as a function of detector position. The global target transmission ratio $\Sigma T/\Sigma M$ increases with decreasing energy.

The second step of the data analysis used the previously selected statistics in order to check the stability of the neutron detectors, to determine the parameters of the statistical distribution and to obtain the final results. The ratios of monitor and transmission detector

Table 1. Total statistics over the run for each neutron detector M1, M2, T1–T3 at different neutron beam energies and P_T signs. The count numbers for each detector are given in 10^6 units. Here, $\Sigma T/\Sigma M = 2 \cdot (T1 + T2 + T3)/3 \cdot (M1 + M2)$. The energy in the BT centre is given

T_{kin}	P_T	Statistics of detectors					$\sum T/\sum M$
(GeV)	sign	M1	M2	T1	T2	T3	
1.59	+	10.0	9.89	8.80	8.45	7.94	0.844
1.79	+	15.63	15.32	13.43	12.88	12.19	0.829
1.79	−	24.53	24.04	20.71	20.16	18.95	0.821
2.10	+	32.02	31.09	26.81	24.80	24.32	0.802
2.10	−	35.81	34.74	29.44	28.26	27.24	0.803

rates as functions of time were obtained and analysed for each neutron energy and the P_T sign. No significant time dependence of the checked values was observed.

The results were extracted using two relations (2.5a) and (2.5b). Each of them contains a hidden contribution from the instrumental asymmetry (IA) due to counter misalignments and the perpendicular components in the beam polarization. The θ and ϕ symmetries of beam neutron charge-exchange reactions in the radiators and scintillators can be strongly violated. On the other hand, the instrumental asymmetry contributions provided by the PPT are fairly negligible due to a large distance from the transmission modules. Assuming that only the measured values of $\Delta\sigma_{L,T}$ depend on the $\vec{P}_T$ direction, the $\Delta\sigma_{L,T}$ and IA effects are either added or subtracted in Eqs.(2.5a,b). For this reason, the half-sum from Eq.(2.7), i.e., a simple average, provides $\Delta\sigma_{L,T}$ whereas the half-difference gives the value of IA , as discussed in [41]. Using such a manner of obtaining the final $\Delta\sigma_{L,T}$ results, the IA contribution could be hardly suppressed.

Due to the longitudinal $\vec{P}_B$ direction and full axial symmetry, the IA is usually small for the $\Delta\sigma_L$ experiment. It can be very large for the $\Delta\sigma_T$ measurement, where no symmetry exists. One can see that the results strongly depend on the detector stabilities and their fixed positions over the data acquisition with both P_T signs. For stable detectors, a pure $\Delta\sigma_{L,T}$ effect is expected to be time-independent and equal for each transmission detector, within statistical errors. In contrast, the value of IA depends on each individual neutron detector, including the monitors.

The $-\Delta\sigma_L(np)$ values for both signs of P_T, their half differences and half-sums are listed in Table 2. All the results were obtained using common statistics from both monitors M1 and M2. Abreviation T1,2,3 signifies that the entire statistics from all the T-detectors were taken into account.

One can see that the IA was much smaller for modules T1 and T3 than for module T2. The IA values change their sign for almost all modules between 1.79 and 2.20 GeV. Since

Table 2. The measured $-\Delta\sigma_L(np)$ values at different energies in the PPT centre for the two opposite target polarizations, for individual transmission detectors and for the cumulated statistics. Instrumental asymmetry (IA) and the averaged $-\Delta\sigma_L(np)$ data are deduced. The quoted errors are statistical only

T_{kin} (GeV)	Transm. detectors	$-\Delta\sigma_L(P_T^+)$ (mb)	$-\Delta\sigma_L(P_T^-)$ (mb)	IA (mb)	Average $-\Delta\sigma_L$ (mb)
1.59	T1	$+4.70 \pm 3.85$			$+4.70 \pm 3.85$
	T2	$+5.45 \pm 3.90$			$+5.45 \pm 3.90$
	T3	$+1.96 \pm 3.99$			$+1.96 \pm 3.99$
	T1,2,3	$+4.07 \pm 2.85$			$+4.07 \pm 2.85$
1.79	T1	$+0.71 \pm 3.03$	$+2.52 \pm 2.29$	-0.90 ± 1.90	$+1.62 \pm 1.90$
	T2	-4.17 ± 3.07	$+0.22 \pm 2.31$	-2.20 ± 1.92	-1.97 ± 1.92
	T3	-0.93 ± 3.13	-0.28 ± 2.36	-0.32 ± 1.96	-0.60 ± 1.96
	T1,2,3	-1.45 ± 2.24	$+0.85 \pm 1.68$	-1.15 ± 1.40	-0.30 ± 1.40
2.20	T1	$+3.43 \pm 2.07$	$+2.00 \pm 1.82$	$+0.72 \pm 1.38$	$+2.71 \pm 1.38$
	T2	$+4.05 \pm 2.13$	-2.02 ± 1.85	$+3.03 \pm 1.41$	$+1.01 \pm 1.41$
	T3	-0.07 ± 2.14	$+0.35 \pm 1.88$	-0.21 ± 1.42	$+0.14 \pm 1.42$
	T1,2,3	$+2.50 \pm 1.53$	$+0.13 \pm 1.34$	$+1.19 \pm 1.02$	$+1.31 \pm 1.02$

the elements of the detectors were not moved during the run, we assume that the residual perpendicular components in $\vec{P}_B$ were opposite.

Relative normalization and systematic errors from different sources are summarized as follows:

Beam polarization including time dependence	$\pm$ 1.7 %
Target polarization	$\pm$ 5.0 %
Number of the polarizable hydrogen atoms including a filling mode	$\pm$ 1.5 %
Neutron spin rotator	$\pm$ 0.2 %
Polarization of other atoms	$\pm$ 0.3 %
Inefficiencies of veto counters	$\pm$ 0.1 %
Total of relative systematic errors	$\pm$ 5.5 %
Absolute error due to the extrapolation of the $-\Delta\sigma_L(np)$ results towards $\Omega = 0$	< 0.04 mb

6. RESULTS AND DISCUSSION

The final $-\Delta\sigma_L(np)$ values are presented in Table 3 and Fig 3. The statistical and systematic errors are quoted. The total errors are the quadratic sums of both uncertainties. As the measurement at 1.59 GeV was carried out with one sign of P_t only, the instrumental ϕ-asymmetry could not be removed using Eq.(2.7). For this energy, we added the weighted average of the absolute IA values at 1.79 and 2.20 GeV ($\pm$ 1.18 mb) in quadrature to the overall systematic error.

The results from Refs.3,4,5 together with the existing $\Delta\sigma_L(np)$ data [17-21], obtained with free polarized neutrons at lower energies, are also shown in Fig. 3. We can see that the new results are smoothly connected with the lower energy data and confirm a fast decrease to zero within a 1.2-2.0 GeV energy region, observed previously [3,4,5].

The solid curves show the last energy-dependent GW/VPI-PSA [26] fits (SAID FX98 and SP99 solutions) of this observable over the interval from 0.1 to 1.3 GeV. Note that the present GW/VPI-PSA np database contains the JINR $\Delta\sigma_L(np)$ result at 1.2 GeV [3,4,5]. Above 1.1 GeV (SATURNE II), the np database is insufficient and a high energy part of the $\Delta\sigma_L(np)$ predictions [26] still disagrees with the measured data. Note that no extrapolation is allowed out of the region of the PSA validity. Concerning pp elastic scattering, the GW/VPI-PSA covers an energy range of up to 2.55 GeV and the SG-PSA up to 2.7 GeV. Both PSA contain almost all existing NN data. Data of the ANL-ZGS scattering experiments together

Table 3. The final $-\Delta\sigma_L(np)$ results. The total errors are quadratic sums of the statistical and systematic ones. The energy and laboratory momenta of the neutron beam correspond to the production target centre

T_{kin} (GeV)	p_{lab} (GeV/c)	$-\Delta\sigma_L(np)$ (mb)	Statis. error (mb)	System. error (mb)	Total error (mb)
1.59	2.35	+4.07	$\pm$2.85	$\pm$1.20	$\pm$3.10
1.79	2.56	−0.30	$\pm$1.40	$\pm$0.02	$\pm$1.40
2.20	2.99	+1.31	$\pm$1.02	$\pm$0.07	$\pm$1.02

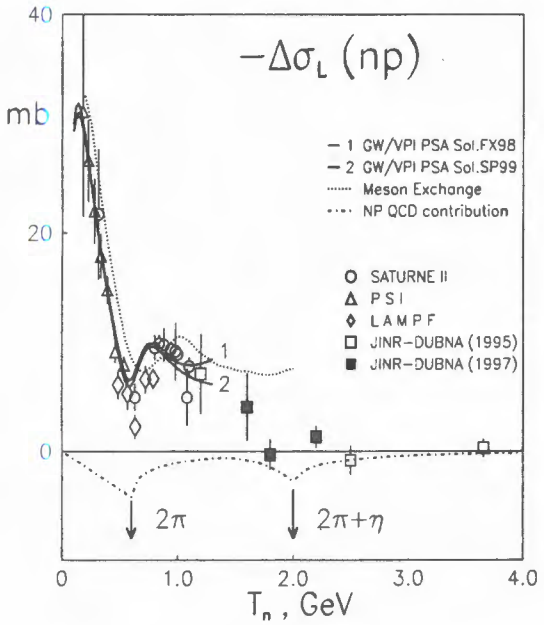

Fig. 3. Energy dependence of the $-\Delta\sigma_L(np)$ observable obtained with free neutron polarized beams. The curves are explained in the text

Table 4. The $-\Delta\sigma_L(I=0)$ values deduced from the present $\Delta\sigma_L(np)$ results and existing $\Delta\sigma_L(pp)$ data. The energies of $\Delta\sigma_L(pp)$ data and corresponding references are also listed

$T_{\rm kin}(np)$ (GeV)	$T_{\rm kin}(pp)$ (GeV)	$-\Delta\sigma_L(pp)$ (mb)	Ref. pp	$-\Delta\sigma_L(I=0)$ (mb)
1.59	1.594	$+4.93 \pm 0.30$	[47]	$+3.2 \pm 6.2$
1.79	1.798	$+3.39 \pm 0.10$	[47]	-4.0 ± 2.8
2.20	2.176	$+2.28 \pm 0.10$	[43]	$+0.3 \pm 2.0$

with the $\Delta\sigma_L(pp)$ results [42,43,44] allowed one to perform the fixed energy PSA at 6 and 12 GeV/c [45,46].

Using Eq.(2.12), one can deduce the values of $\Delta\sigma_L(I=0)$ from the obtained $\Delta\sigma_L(np)$ results and the existing $\Delta\sigma_L(pp)$ data. For this purpose, we used the ANL-ZGS [43] and SATURNE II [47] $\Delta\sigma_L(pp)$ data. The results are given in Table 4 and in Fig. 4. Since the pp data are accurate, the values of $-\Delta\sigma_L(I=0)$ have roughly two times larger errors than the obtained np results. For this reason, an improved accuracy of np measurements is important.

The values of $-\Delta\sigma_L(I=0)$ from [3,4,5] together with the ones using the $\Delta\sigma_L(np)$ data sets [17-21] are also plotted in Fig. 4. All the results are compatible and suggest a shoulder or a maximum over a region of 1.2-1.6 GeV followed by a rapid decrease with increasing energy. The solid curves represent the recent GW/VPI-PSA [26] (SAID FX98 and SP99) energy-dependent predictions for $-\Delta\sigma_L(I=0)$. In addition, the $-\Delta\sigma_L(I=1)$ fit SAID SP99 is also shown. It should be noted that the $\Delta\sigma_L(pp)$ data set is richer in the energy

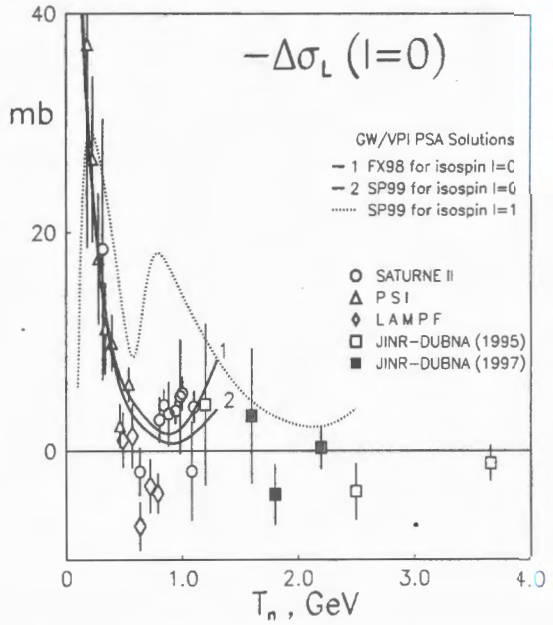

Fig. 4. Energy dependence of the $-\Delta\sigma_L(I=0)$. The notation is the same as in Fig.3

region of interest and the continuation of the $\Delta\sigma_L(np)$ measurements in Dubna is highly desirable to obtain the $\Delta\sigma_L(I=0)$ quantities at energies corresponding to the pp data.

A number of dynamic models have predicted the $\Delta\sigma_{L,T}$ energy behaviour for np and pp interactions. Below 2.0 GeV, a usual meson exchange theory of NN scattering [48] gives the $\Delta\sigma_L(np)$ energy dependence as shown by the dotted curve in Fig. 3. It can be seen that this model provides a qualitative description only.

Another dynamic model prediction for the $\Delta\sigma_L(np)$ energy dependence was discussed in [3,4,5]. This prediction concerns a contribution to the $\Delta\sigma_L(np)$ value from nonperturbative flavour-dependent interaction between quarks, induced by a strong fluctuation of vacuum gluon fields, i.e., instantons (see, for example [49,50,51]). An anomalous energy dependence of the instanton-induced interaction near 2π and $2\pi+\eta$ thresholds leads to large contributions of this mechanism to spin-dependent cross sections. A qualitatively estimated contribution of the instanton-induced interaction to the $\Delta\sigma_L(np)$ energy dependence is shown in Fig.3 by a dashed line.

The investigated energy region corresponds to a possible generation of heavy dibaryons with masses $M > 2.4$ GeV (see review [52]). For example, the model [53,54] predicts the formation of a heavy dibaryon state with a colour octet-octet structure.

A possible manifestation of exotic dibaryons in the energy dependence of different pp and np observables was predicted by another model [55-59]. The authors used the Cloudy Bag Model and R matrix to connect a long-range meson-exchange force region with a short-range region of asymptotically free quarks. The model gives the lowest lying exotic six-quark configurations in the isosinglet and spin-triplet state $^3S_1$ with M = 2.63 GeV (T_{kin} = 1.81 GeV). The $^3S_1$ partial wave is expected to be predominant for the $I=0$ state. The measurements of the $\Delta\sigma_{L,T}$ observables for np and the determination of the $\Delta\sigma_{L,T}(I=0)$

quantities can provide a significant check for the predicted dibaryon. Since $\Delta\sigma_T$ for an arbitrary isospin state contains no uncoupled spin-triplet, a possible dibaryon resonance effect in $^3S_1$ can be less diluted. Moreover, the spin-singlet contribution vanishes in the difference of both quantities.

The three optical theorems determine the imaginary parts of the nonvanishing forward amplitudes as shown in Eqs.(2.8) to (2.10). A maximum in the $I = 0$ amplitudes or their combinations dominanted by a spin triplet, is a necessary condition for the predicted resonance. A sufficient condition can be provided by real parts. For np scattering, they can be determined by measuring observables in the experimentally accessible backward direction, as shown in [60].

The $I = 0$ spin-dependent total cross sections represent a considerable advantage for studies of possible resonances. This is in contrast with the $I = 1$ system where the lowest lying exotic six-quark configuration corresponds to the spin-singlet state $^1S_0$. This state is not dominant, and it is hard to separate it in the forward direction. Scattering data directly related with the spin-singlet amplitude at other angles are preferable to be measured.

7. CONCLUSIONS

The new results are presented for the transmission measurements of the -$\Delta\sigma_L(np)$ energy dependence in the Dubna Synchrophasotron energy region below 3.7 GeV. The measured values of -$\Delta\sigma_L(np)$ are compatible with the existing np results, using free neutrons. A rapid decrease of the $-\Delta\sigma_L(np)$ values from 1.1 to 2.0 GeV is confirmed.

The $-\Delta\sigma_L(I = 0)$ quantities, deduced from the measured values of $-\Delta\sigma_L(np)$ and the existing $\Delta\sigma_L(pp)$ data are also presented. They indicate a shoulder or a maximum over a region of 1.2-1.6 GeV followed by a rapid decrease with energy.

The obtained results are compared with the dynamic models predictions and the recent GW/VPI-PSA fits. The necessity of further $\Delta\sigma_L(np)$ measurements and new $\Delta\sigma_T(np)$ data over a kinetic energy region above 1.1 GeV is emphasized.

ACKNOWLEDGEMENTS

The authors thank the JINR LHE and LNP Directorates for their support of these investigations. Discussions with V.N.Penev have solved several problems. We are grateful to J.Ball, M.P.Rekalo and I.I.Strakovsky for helpful suggestions.

The measurements were possible due to the JINR Directorate Grant. The work was in part supported by the International Science Foundation and Russian Government through Grant No. JHW 100, the International Association for the Promotion of Cooperation with Scientists from the Independent States of the Former Soviet Union (INTAS) through Grant No. 93-3315, the Russian Foundation for Basic Research through Grants RFBR-93-02-03961, RFBR-93-02-16715, RFBR-95-02-05807, RFBR-96-02-18736 and the Fundamental Nuclear Physics Foundation Grant 122.03.

References

1. Ball J. et al. — In: Proc.Int.Workshop "Dubna Deuteron-91", JINR, E2-92-25, Dubna, 1992, p.12.
2. Cherhykh E. et al. — In: Proc. Int. Workshop "Dubna Deuteron-93", JINR, E2-94-95, Dubna, 1994, p.185;
   Proc. "V Workshop on High Energy Spin Physics", Protvino, 20-24 September 1993, Protvino, 1994, p.478.
3. Averichev S.A. et al. — In: Proc.of "VI Workshop on Spin Phenomena in High Energy Physics", Protvino, September 18-23, 1995, Protvino, 1996, v.2, p.63.
4. Adiasevich B.P. et al. — Zeitschrift für Physik, 1996, C71, p.65.
5. Sharov V.I. et al. — JINR Rapid Communications, 1996, No.3[77]-96, p.13.
6. Lehar F. et al. — Nucl. Instrum. Methods, 1995, v.A356, p.58.
7. Bazhanov N.A. et al. — Nucl. Instrum. Methods, 1996, v.A372, p.349.
8. Issinsky I.B. et al. — Acta Physica Polonica, 1994, v.B25, p.673.
9. Kirillov A. et al. — JINR Preprint E13-96-210, Dubna, 1996.
10. Chernykh E.V., Zaporozhets S.A. — Proceedings of the ESONE International Conference "RTD 94". Editors R.Pose, P.U. ten Kate, E.W.A.Lingeman; JINR Preprint E10,11-95-387, Dubna, 1995, p.179.
11. Anischenko N.G. et al. — JINR Rapid Communications, 1998, No.6[92]-98, p.49.
12. Sharov V.I. et al. — In: "Proceedings of VII Workshop on High Energy Spin Physics. SPIN-97.", July 7-12, 1997, Dubna, Russia. Editted by Efremov A.V., Selyugin O.V. JINR, E2-97-413, Dubna 1997, p.263.
13. Grosnick D.P. et al. — Phys. Rev., 1997, v.D55, p.1159.
14. Lechanoine-Leluc C., Lehar F. — Rev. Mod. Phys., 1993, v.65, p.47.
15. Auer I.P. — Phys. Rev. Lett., 1981, v.46, p.1177.
16. Grein W., Kroll P. — Nucl. Phys., 1982, v.A377, p.505.
17. Lehar F. et al. — Phys. Lett., 1987, v.189B, p.241.
18. Fontaine J.-M. et al. — Nucl. Phys., 1991, v.B358, p.297.
19. Ball J. et al. — Zeitschrift für Physik, 1994, v.C61, p.53.
20. Binz R. et al. — Nucl. Phys., 1991, v.A533, p.601.
21. Beddo M. et al. — Phys. Lett., 1991, v.258B, p.24.

22. Haffter P. et al. — Nucl. Phys., 1992, v.A548, p.29.

23. Brož J. — Zeitschrift für Physik, 1997, v.A359, p.23.

24. Wilburn W.S. et al. — Phys. Rev., 1995, v.C52, p.2353.

25. Brož J. et al. — Zeitschrift für Physik, 1997, v.A355, p.401.

26. Arndt R.A. et al. — Phys. Rev., 1997, v.C56, p.3005.

27. Bystrický J., Lehar F., Winternitz P. — J.Physique (Paris), 1978, v.39, p.1.

28. Bilenky S.M., Ryndin R.M. — Phys. Lett., 1963, v.6, p.217.

29. Phillips R.J.N. — Nucl. Phys., 1963, v.43, p.413.

30. Ball J. et al. — Nuovo Cimento, 1998, v.A111, p.13.

31. Bystrický J., Lechanoine-LeLuc C., Lehar F. — Eur. Phys.J., 1998, v.C4, p.607.

32. Ableev V.G. et al. — Nucl. Instrum. Methods, 1991, v.A306, p.73.

33. Azhgirey L.S. et al. — Pribory i Tekhnika Experimenta, 1997, v.1 p.51; Transl. Instrum. and Exp. Techniques, 1997, v.40, p.43.

34. Bazhanov N.A. et al. — Nucl. Instrum. Methods, 1998, v.A402, p.484.

35. Ableev V.G. et al. — Nucl. Phys., 1983, v.A393, p.941 and 1983, v.A411, p.541E.

36. Cheung E. et al. — Phys. Lett., 1992, v.B284, p.210.

37. Nomofilov A.A. et al. — Phys. Lett., 1994, v.B325, p.327.

38. Ghazikhanian V. et al. — Phys. Rev., 1991, v.C43, p.1532.

39. Bunyatova E.I., Galimov R.M., Luchkina S.A. — JINR Preprint 12-82-732, Dubna, 1982.

40. Barashenkov. V.S. — *"Secheniya vzaimodeistviya chastits i yader s yadrami"*. JINR, Publishing Department, Dubna, 1993.

41. Perrot F. et al. — Nucl. Phys., 1986, v.B278, p.881.

42. Auer I.P. et al. — Phys. Lett., 1977, v.B70, p.475.

43. Auer I.P. et al. — Phys. Rev. Lett., 1978, v.41, p.354.

44. Auer I.P. et al. — Phys. Rev. Lett., 1989, v.62, p.2649.

45. Matsuda M., Suemitsu H., Watari W., Yonezawa M. — Prog. Theor. Phys., 1979, v62, 1436; 1980, v.64, 1344; 1981, v.66, p.1102.

46. Matsuda M., Suemitsu H., Yonezawa M. — Phys. Rev., 1986, v.D33, p.2563.

47. Bystrický J. et al. — Phys.Lett., 1984, v.142B, p.130.

48. Lee T.-S.H. — Phys. Rev., 1984, v.C29, p.195.

49. 't Hooft G. — Phys. Rev., 1976, v.D14, p.32.

50. Dorokhov A.E., Kochelev N.I., Zubov Yu.A. — Int. J. Mod. Phys., 1993, v.A8, p.603.

51. Dorokhov A.E., N.I.Kochelev — Sov. J. Part. Nucl., 1995, v.26, p.5.

52. Strakovsky I.I. — Fiz. Elem. Chastits At. Yadra, 1991, v.22, p.615; Transl. Sov. J. Part. Nucl., 1991, v.22, p.296.

53. Kopeliovich B.Z., Niedermayer F. — Zh. Eksp. Teor. Fiz., 1984, v.87, p.1121; Transl. Sov. Phys. JETP, 1984, v.60 (4), p.640.

54. Kopeliovich B.Z. — Fiz. Elem.Chastits At. Yadra, 1990, v.21, p.117; Transl. Sov. J. Part. Nucl., 1990, v.21 (1), p.49.

55. LaFrance P., Lomon E.L. — Phys. Rev., 1986, v.D34, p.1341.

56. Gonzales P., LaFrance P., Lomon E.L. — Phys. Rev., 1987, v.D35, p.2142.

57. LaFrance P. — Can. J. Phys., 1990, v.68, p.1194.

58. Lomon E.L. — Colloque de Physique (France), 1990, v.51, p.C6-363.

59. LaFrance P., Lomon E.L. — Proceedings of the International Conference "Mesons and Nuclei at Intermediate Energies", Dubna, 3-7 May 1994. Editors: Khankhasaev M.Kh. and Kurmanov Zh.B. World Scientific. Singapore, 1995-XV, p.97.

60. Ball J. — Eur. Phys. J., 1998, v.C5, p.57.

Received on August 13, 1999.

УДК 539.172.17

TO THE ESTIMATION OF ANGULAR DISTRIBUTIONS OF DOUBLE CHARGED SPECTATOR FRAGMENTS IN NUCLEUS-NUCLEUS INTERACTION AT SUPERHIGH ENERGIES

A.I.Bondarenko[1], *V.V.Uzhinskii*[2]

The pseudo-rapidity distributions of double charged spectator fragments produced in the interactions of ^{12}C, ^{22}Ne, ^{24}Mn, ^{28}Si (4,5 GeV/c/nucleon), and ^{56}Fe (2,5 GeV/c/nucleon) with nuclear photoemulsion are studied experimentally. It is shown that the width of the distribution does not depend practically on the mass number of fragmenting nucleus and beam energy. The centre of the distribution is correlated with beam energy. All this allows one to estimate the angular distributions of fragments in superhigh energy nuclear collisions.

The investigation has been performed at the Laboratory of Computing Techniques and Automation, JINR.

К оценке угловых распределений двухзарядных спектаторных фрагментов в ядро-ядерных взаимодействиях при сверхвысоких энергиях

А.И.Бондаренко, В.В.Ужинский

Экспериментально исследуются псевдобыстротные распределения двухзарядных спектаторных фрагментов, рождающихся во взаимодействиях ^{12}C, ^{22}Ne, ^{24}Mn, ^{28}Si (4,5 ГэВ/с/нуклон) и ^{56}Fe (2,5 ГэВ/с/нуклон) с ядрами фотоэмульсии. Показано, что ширина распределения практически не зависит от массы фрагментирующих ядер и от энергии пучка. Положение центра распределения коррелирует с энергией пучка. Все это позволяет оценить угловые распределения фрагментов при сверхвысоких энергиях.

Работа выполнена в Лаборатории вычислительной техники и автоматизации ОИЯИ.

To study nucleus-nucleus interactions at superhigh energies, it is assumed to use different detectors of singly charged relativistic particles. The possibility of multi-charged nuclear fragment penetration through such a detector and its response are not usually considered. It is supposed that the nuclear fragments will fly at small angles to the beam direction and will

[1]INP, Tashkent, Uzbekistan
[2]E-mail: UZHI@CV.JINR.DUBNA.SU

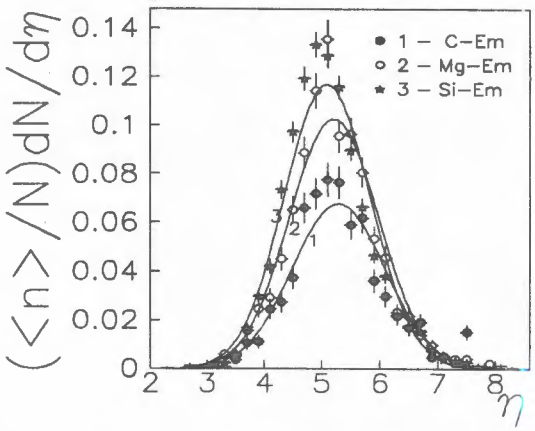

Fig. 1. Pseudo-rapidity distributions of double charged fragments in ^{12}C, ^{24}Mg, ^{28}Si + Em interactions

not enter the designed installations. Our paper is aimed to give the possibility to check up the hypothesis.

It is clear that one needs to know the distributions of nuclear fragments on kinematic variables in order to check the hypothesis. The kinematic characteristics of the fragments are studied thoroughly at low and intermediate energies. Though, these data cannot be used because there is a strong overlap of fragmentation regions of colliding nuclei at such energies.

At high energies ($E/A > 1$ GeV), there is only a restricted set of experimental data (see, e.g., [1, 2]). The needed data can be obtained from emulsion experiments. Such data were presented in Ref. 3 for gold interactions with emulsion nuclei at an energy of 10.6 GeV/nucleon. According to Ref. 3, the widths of the pseudo-rapidity distributions for double-charged, light ($3 \leq Z \leq 5$) and heavy ($Z \geq 6$) fragments are equal to 1, 1, and 3, respectively. The distribution characteristics in other interactions are unknown.

Below, we present the main characteristics of double-charged fragment pseudo-rapidity distributions in the interactions of ^{12}C, ^{24}Mg, ^{28}Si at an energy of 3.7 GeV/nucleon, ^{14}N at an energy of 2.1 GeV/nucleon, and ^{56}Fe at an energy of 1.7 GeV/nucleon with nuclear photoemulsion. The data were obtained in the experiments identical in development selection and identification of spectator fragments of projectile nuclei (see Refs. 4-8).

Figure 1 shows the pseudo-rapidity distributions of double-charged fragments in ^{12}C, ^{24}Mg, ^{28}Si + Em interactions. Here $\eta = -\ln \mathrm{tg}\,\theta/2$, where θ is the polar angle of a fragment measured from the beam direction.

As one can see, the distributions for different fragmenting systems are alike. Such quantitative characteristics of the distributions as the standard deviation ($D = \sqrt{< \eta^2 > - < \eta >^2}$), mean value of pseudo-rapidity ($< \eta >$), and multiplicity of double-charged fragments are given in the Table.

According to the Table, the characteristics of the distributions depend on interaction energy, the type of projectile and target nuclei. The distributions differ from the gaussian ones (see the solid curves calculated using the data presented in the Table). Only in a rough approximation, one can assume that the width of the distributions is the same as the mean values of pseudo-rapidity at a fixed interaction energy.

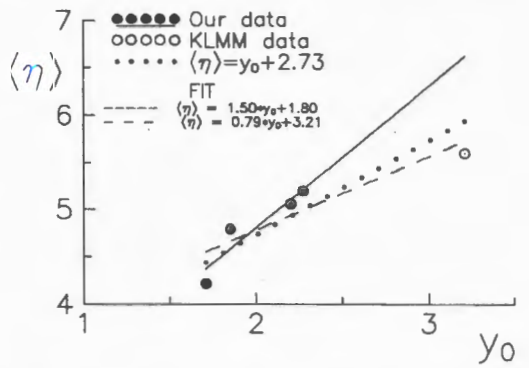

Fig. 2. Mean value of double charged fragment pseudo-rapidity distribution as a function of beam rapidity

One can understand some specific features of the distributions assuming that the rapidities of the fragments (y) are equal to the rapidity of the incident nucleus. Then at high energies one gets

$$y = \frac{1}{2} \ln \frac{E + P_z}{E - P_z} \simeq \eta - \frac{m^2}{2p_T^2},$$

where m, E, p_z, and p_T are the mass, energy, longitudinal and transversal momentum of the fragment, respectively. As far as we know, the transversal momentum distributions of fragments depend weakly on energy, so $< \eta >$ must be in straightline proportion to the rapidity of projectile nucleus. The data of Fig. 2 are not contradictory to this conclusion.

Table. Main characteristics of the pseudo-rapidity distributions

Ensemble	p_0, GeV/c/nucleon	$\langle n_\alpha \rangle$	$\langle \eta_\alpha \rangle$	$\sigma(\eta_\alpha)$
^{12}C – Em	4.5	0.68 ± .02	5.29 ± .02	.81 ± .02
^{24}Mg – Em	4.5	0.99 ± .02	5.21 ± .02	.77 ± .01
^{28}Si – Em	4.5	1.08 ± .02	5.09 ± .01	.74 ± .01
^{56}Fe – H	2.5	1.29 ± .06	4.34 ± .02	.64 ± .02
^{56}Fe – CNO	2.5	1.64 ± .07	4.27 ± .02	.73 ± .02
^{56}Fe – AgBr	2.5	1.75 ± .05	4.15 ± .02	.75 ± .01
^{22}Ne – Em	4.2	0.82 ± .02	5.06 ± .01	.77 ± .01
^{14}N – Em	2.9	0.74 ± .03	4.79 ± .03	.84 ± .02
^{56}Fe – Em	2.5	1.65 ± .04	4.22 ± .01	.74 ± .01

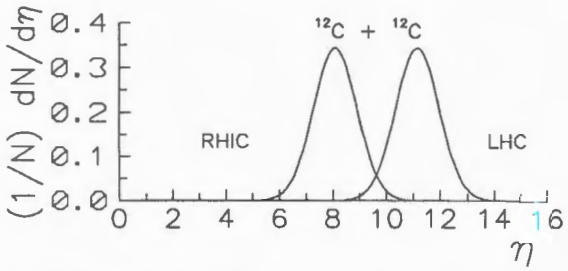

Fig. 3. Pseudo-rapidity distributions of double charged fragments in nucleus-nucleus interactions at superhigh energies

The mentioned properties of the distributions allow one to make predictions for superhigh energies. Figure 3 gives the calculated distributions of double-charged fragments in $^{12}C + ^{12}C$ interactions at $\sqrt{s_{NN}} = 200$ and 5000 GeV. In principle, they can be checked up with extracted beams of superhigh energy nuclei.

The authors are thankful to P.G. Zarubin for stimulating discussion.

References

1. Baldin A.M. — Fiz. Elem. Chastits At. Yadra, 1977, v.8, p.429.
2. Karnaukhov V.A. et al. — JINR Prep. E7-95-321, Dubna, 1995; JINR Prep. E1-96-50, Dubna, 1996;
   Shmakov S.Yu. et al. — Yad. Fiz., 1995, v.58, p.1735 (Phys. At. Nucl. (Engl. Transl.), v. 58, p. 1635).
3. KLMM Collab. (Cherry M.L. et al.) — Phys. Rev., 1995, v. C52, p. 2652.
4. Bondarenko A.I. et al. — Izv. AN UzSSR. ser. fiz.-mat. nauk, 1979, N2, p. 73.
5. Ameeva B.U. et al. — Yad. Fiz., 1988, v.47, p. 949.
6. Bondarenko A.I. et al. — Yad. Fiz., 1992, v.55, p.137.
7. Bondarenko R.A. et al. — Doklady AN Uz.SSR, 1991, N3, p.29;
8. Chernov G.M. et al. — Nucl.Phys., 1984, v.A412, p.534.
9. Adamovich M.I. et al. — Phys.Rev., 1989, v.C40, p.66.

Received on August 8, 1999.

УДК 539.1.074.55

SIMULATION dE/dx ANALYSIS RESULTS FOR SILICON INNER TRACKING SYSTEM OF ALICE SET-UP AT LHC ACCELERATOR

B.Batyunya

The particle identification by using dE/dx analysis in the ALICE silicon Inner Tracking System (ITS) was studied by simulations. Correction procedures were considered and used to improve charge collection and resolution. Particle identification efficiencies and contamination rates depending on the function of momentum were obtained by the probability weight calculation for each particle species ($\pi^{\pm}$, $K^{\pm}$, $p/\overline{p}$).

The investigation has been performed at the Laboratory of High Energies, JINR.

Результаты dE/dx анализа моделированных событий для силиконовой внутренней трековой системы установки ALICE ускорителя LHC

Б.В.Батюня

С помощью моделирования исследована возможность идентификации частиц по потерям энергии в силиконе (из dE/dx анализа) для силиконовой внутренней трековой системы установки ALICE. Рассмотрены некоторые процедуры коррекции потерь заряда, позволяющие улучшить разрешение по заряду и информацию о полном заряде, образующемся при прохождении частиц через силиконовые слои. Определены эффективности идентификации частиц и доли примеси (как функции импульса частиц) посредством вычисления вероятностных весов для частиц каждого сорта ($\pi^{\pm}$, $K^{\pm}$, $p/\overline{p}$).

Работа выполнена в Лаборатории высоких энергий ОИЯИ.

1. INTRODUCTION

The mesurement of the energy loss in thin silicon detectors can be used for particle identification (PID) in the nonrelativistic ($1/\beta^2$) region. This ionization information may be combined with the TPC one and with the TOF measurements to improve the quality and the range over which the PID can be done. Besides, this information is unique in the ALICE ITS for the slow tracks which do not reach the outer detectors because of decays, energy loss or curling but the tracking and momentum resolution is possible with six silicon layers of the ITS. Some simulation of PID for the ALICE ITS has been presented in the ALICE TP (see Section 11.4.1 in [1]). In this note more detailed simulation analyses were carried out and the separation power was defined for charged hadrons (pions, kaons, protons) in different momentum regions with the aid of PID weights obtained for each particle.

2. DETECTOR SIMULATION

The detailed simulation model (in the frame of GEANT) is described in Refs. 2,3 . Some detector parameters have been modified with respect to the ALICE TP (see Sect. 2.1 of [1]). The two pixel layers were not considered since they are digital devices, for the dE/dx analysis. We considered two layers of silicon drift detectors (SDD) with anode pitch of 210 μm, and a drift direction transverse to the beam line; and two layers of double-sided microstrip detectors (SSD) with a strip pitch of 95 μm and a stereo angle of 30 mrad. Some details for the mechanical support and cooling systems and the beam pipe were included also in the simulation. The overall matter budget was 5.5%(X/X_0) and consisted of:

- 0.28%(X/X_0) for the beam pipe,
- 1.50%(X/X_0) for two pixel layers,
- 1.66%(X/X_0) for two SDD layers,
- 1.42%(X/X_0) for two double-sided strip layers,
- 0.72%(X/X_0) for outer shell.

3. CHARGE COLLECTION AND ANALYSIS

The GEANT procedure generates charge (energy loss) Landau distribution for each single hit and, in general, this charge is collected in a number of anodes/strips (i.e., a cluster is

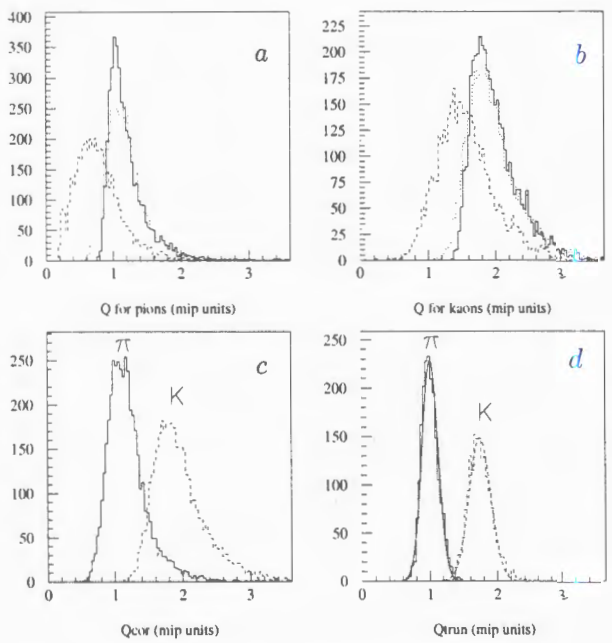

Fig. 1. Charge distributions for π and K in the momentum interval (470÷530) MeV/c (the different distributions are explained in the text)

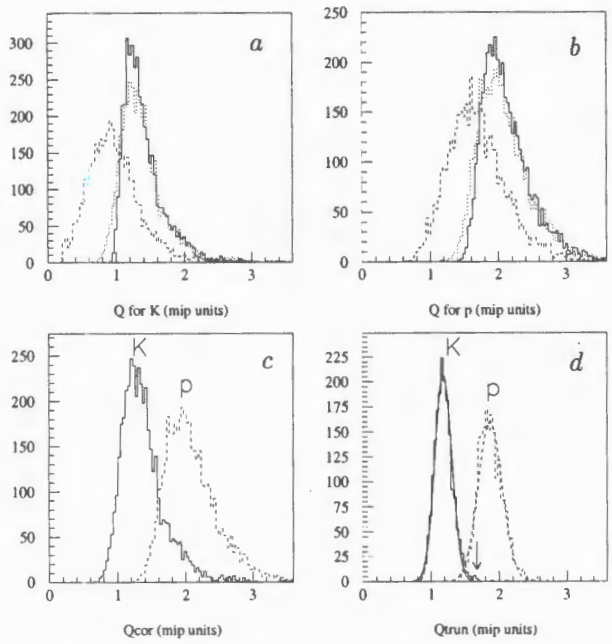

Fig. 2. Charge distributions for K and protons in the momentum interval (830÷930) MeV/*c* (the different distributions are explained in the text)

produced) [3]). In this case a variable fraction of the charge can be lost below a noise threshold if zero suppressed data are used. The charge loss depending on the cluster size is most important for the SDD and very small for the SSD. In Ref. 3, a special correction function was suggested that is used in the present analysis. The second problem relates to the fact that the charge value depends not only on particle kind and momentum but also on the path length inside the silicon (depending on the angle of particle). A correction for this effect has been done in addition.

Figs.1*a* and *b* show (for the SDD) the charge distributions generated with the GEANT package (solid lines), those obtained from the cluster analysis with due account of the noise but without the correction (dashed lines), and after the correction function using (dotted lines). The charge unit is taken as minimum particle ionization (1 mip is 20500 e^-). The distributions have been obtained for π^+ and K^+ in the momentum region of 470÷530 MeV/*c* (2000 particles of each kind have been generated). The same distribution but for K^+ and protons at the momenta of 830÷930 MeV/*c* is shown in Figs.2*a* and *b*. A strong influence of the charge threshold cut and a satisfactory result of the correction procedure is observed. It should be noted that a pessimistic noise value with σ_{noise} = 500 e^- was used for the simulation (the threshold was taken of $3\times\sigma_{noise}$), and in some realistic case, for example for OLA electronics, the equivalent noise charge was measured to be $\simeq$ 230 e^- ([4]) and the shift of the charge distributions in Figs.1(a, b) and Figs.2(a, b may be decreased by a factor of nearly 1.4. On the other hand, a real experimental test of the charge collection is under study now. For example, the analysis of the nonzero-suppressed data leads to the independence of

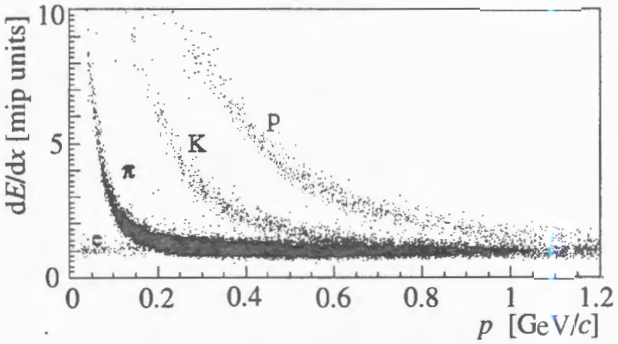

Fig. 3. Energy loss — momentum scatter plot for four silicon layers of ALICE ITS and for different particles (e, π, K, p)

the collected charge of the drift time for the SDD (see Fig. 4.5 in Ref. 4), i.e., from the cluster size. Fig.1 *c* and Fig.2 *c* show the charge distributions for particle pairs π,K and K,p in the same narrow momentum regions (for each pairs of particles) considered before. It is seen that Landau distributions are strongly overlapping.

To improve the situation the truncated mean method using the m lowest of n measurements was applied. Only measurements with four or three hits in the ITS were selected ($\simeq$ 90% from all hits, see Sect. 11.4.1 of Ref.1), and the truncated mean was constructed using two out of four or two out of three hits, respectively. The results are shown, for example, in Fig.1 *d* and Fig.2 *d* (see also Sect. 11.4.1 of Ref.1 and Ref.3). One can see that the charge distributions become nearly gaussian (the curves are results of the gaussian fit) and particle separation possibility is much better.

Figure 3 shows charge-momentum scatter plot for the charge (dE/dx) obtained after the corrections and truncated mean procedure for five central Pb-Pb events generated by the HIJING code [5] with a mean rapidity density of charge particles $dN/dy \simeq$ 6000 at y = 0 (gamma conversions and other secondary particle production have been included). Well separated densities are clearly seen for the different particle species.

4. PARTICLE IDENTIFICATION

It is seen from Fig.3 that there are wide enough momentum regions where particles may be separated by simple cuts in the charge, but some additional probability method is necessary if the deposited charges of the different particle kinds are rather similar.To study the situation in more detail the samples of 2000 one-particle-events were generated in subsequent momentum intervals. The intervals were chosen to correspond to $\pm 3\sigma$ of the TPC proton momentum resolution (see Fig.11.9 of [1]), i.e. track reconstruction in the TPC was supposed. At the next step, the charge cuts were chosen if the simple separation is possible or, otherwise, mean charge values ($< q >$) and gaussian fit sigmas (σ_q) were obtained for the next procedure of probability weights (PID weights) calculation.

Table 1 presents the simple charge cut values and information about the PID weights calculation for different momentum regions. "No PID" means that the charge distributions of pions and kaons are practically identical and the particle identification is impossible. Table 2 presents the $< q >$ and σ_q values for kaons and protons in the momentum intervals where

PID weights were calculated. For pions these values are equal to 1.0 mip and 0.12 mip, respectively for all these momentum intervals.

Table 1. Simple charge cut values and information about a need of PID weights calculation for the different momentum intervals

Momentum (MeV/c)	Charge cut (mip)		
	π	K	p
50÷120	all		
120÷200	< 6	≥ 6	
200÷300	< 3.5	3.5÷9	> 9
300÷410	< 1.9	1.9÷4	> 4
410÷470	PID weights		> 3.5
470÷530	– // –		> 3.0
530÷590	no PID		> 2.7
590÷650	– // –		> 2.5
650÷730	– // –		> 2.0
730÷830	– // –		PID weights
830÷930	– // –		– // –
930÷1030	– // –		– // –

Table 2. Mean charge values and sigmas of charge distributions for kaons and protons in the different momentum intervalls

Momentum MeV/c	$< q(K) >$	$\sigma_q(K)$	$< q(p) >$	$\sigma_q(p)$
	(mip)			
410÷470	1.98	0.17		
470÷530	1.75	0.16		
730÷830	1.25	0.13	2.14	0.20
830÷930	1.18	0.125	1.88	0.18
930÷1030	1.13	0.12	1.68	0.155

The PID weights were calculated as follows:

The charge distributions for $\pi^{\pm}$ and $K^{\pm}$ are compared in the momentum regions of (410÷470) and (470÷530) MeV/c and a charge cut equal to a chosen number of $\sigma_q(K)$ is applied to the left from $< q(K) >$ (for example, such a cut is shown by the arrow in Fig.2*d* for K and p). All particles are considered as pions if the charges are below the cut value, otherwise, the PID weights ω_K and ω_π are calculated from the equations:

$\omega_\pi/\omega_K = R_{\pi K}$, $\omega_\pi + \omega_K = 1$ (the normalization),

where $R_{\pi K}$ is defined as a ratio of π and K rates limited by the cut value in the respective charge distributions (the smaller particle rates are taken). As a results, the weights are calculated as:

$\omega_K = 1/(1 + R_{\pi K})$, $\omega_\pi = 1 - \omega_K$.

The weights for protons in the narrow momentum intervals (see Table 1 from 730 MeV/c) are calculated in the same way(π and K are not separated from each other at these momenta). It should be noted that the proton charge distributions have been compared only with the kaon

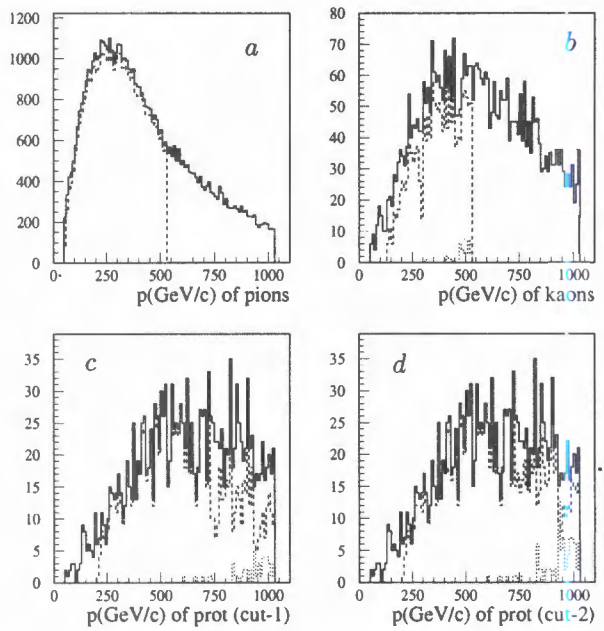

Fig. 4. Momentum distributions for $\pi^{\pm}(a)$, $K^{\pm}(b)$, protons(c and d for cut-1 and cut-2, see text). Solid lines — generated distributions, dashed lined — obtained after ITS simulation and PID procedure (see text), dotted lines — contamination(see text)

ones, since they are always nearer than the pion charge distributions, i.e., the mean proton PID weight is slightly underestimated.

5. RESULTS AND DISCUSSION

The PID procedure described in Sect.3 has been applied for 6 full SHAKER ([6]) events with a charged particle rapidity density of dN/dy = 8000 (at y = 0). All primary particles were generated in polar angle range of 45°÷135° and at the momenta of (0.03÷10.0)GeV/c. The PID weight was obtained for each particle and each momentum interval according to Table 1.

The results are shown in Figs.4(a – d) where the generated momentum spectra (the solid lines) of pions(a), kaons(b) and protons(c, d) are compared with the ones obtained after detector simulation taking into account the PID weights (the dashed lines). Note, that the track reconstruction efficiency was not included, i.e., the particle losses due to interactions, decays, hit numbers smaller than 3 (see Sect.3), and the PID inefficiency due to contamination (the dotted lines in Fig.4) were considered. The first three factors are the most important at the smallest momenta, where significant losses of kaons and protons are observed. The PID inefficiency (the contamination) manifests itself in the regions, where the PID weight calculation is necessary. A cut of -1σ_q(K) has been chosen for π-K separation (see Sect.3) resulting in a total $\pi^{\pm}$ contamination of $K^{\pm}$ of 2%. Figures 4c and d show the results of

proton separation at two cuts of $-1\ \sigma_q$(p) (cut-1) and $-\ 1.5\sigma_q$(p) (cut-2), respectively. The corresponding contamination over the full momentum range, by π/K are 3.5% and 5.8%. It is seen, of course, that when the cut value decreases, both the efficiency of the proton separation and the contamination, increase. The value of the cut applied has to be optimized with respect to the specific physics requirements.

It is necessary to emphasize that the TPC tracking information has been included to this analysis, and that the dE/dx information of the TPC may also be combined to the one of the ITS. The low energy tracking possibility, using the ITS only, is under study now and the corresponding ITS dE/dx analysis will be done in the near future.

6. CONCLUSIONS

The simulation of the particle identification dE/dx analysis in the ALICE ITS has been done, and the particle separation power (PID efficiency and contamination) has been obtained for pions, kaons and protons in narrow momentum intervals between 0.05 and 1.03 GeV/c. The total contamination rates did not exceed 2% for kaons (in the range 150÷530 MeV/c), and (4÷6)% for protons (in the range 200÷1030 MeV/c).

ACKNOWLEDGEMENTS

The author is grateful to P.Giubellino and G.Paić for useful discussions and suggestions.

References

1. Ahmad N. et al. — "ALICE Technical Proposal", CERN/LHCC/95-71, Geneva, 1995.
2. Batyunya B., Zinchenko A. — JINR Communication E1-94-375, Dubna, 1994; Internal Note/SIM ALICE 94-11.
3. Batyunya B., Zinchenko A. — JINR Rapid Communications, 1995, No.3[71]-95, p.5; Internal Note/SIM ALICE 94-31.
4. Bonvicini V. et al. — Internal Note ALICE/98-24.
5. Wang N.X. et al. — Phys. Rev., 1991, v.D44, p.3521; Phys. Rev. Lett., 1992, v.68, 1480.
6. Antinori F. — Internal Note/SIM ALICE/93-09, 1993.

Received on July 30, 1999.

УДК 539.12.01

HIGH-MULTIPLICITY PROCESSES

G.Chelkov, J.Manjavidze*[1], *A.Sissakian

We wish to demonstrate that investigation of asymptotically high multiplicity (AHM) hadron reactions may solve, or at least clear up, a number of problems unsolvable by other ways. We would lean upon the idea: (i) the reactions final state entropy is proportional to multiplicity and, by this reason, just in the AHM domain one may expect the *equilibrium* final state and (ii) the AHM final state is *cold* because of the energy-momentum conservation laws. This means that the collective phenomena may become important in the AHM domain. The possibility of hard *processes* dominance is considered also.

The investigation has been performed at the Laboratory of Nuclear Problems, JINR.

Процессы с большой множественностью

Г.Шелков, И.Манджавидзе, А.Сисакян

Мы хотим показать, что исследование реакций рождения асимптотически большой множественности (АБМ) адронов может решить или, по крайней мере, прояснить, некоторые проблемы, неразрешимые другим образом. Мы собираемся следовать идее: (i) энтропия конечного состояния пропорциональна множественности, и поэтому именно в области АБМ можно ожидать образования равновесного состояния, (ii) конечное состояние с АБМ должно быть холодным в силу сохранения энергии-импульса. Последнее может означать, что в области АБМ коллективные явления могут быть существенны. Рассматривается также вклад жестких процессов при рождении состояния с АБМ.

Работа выполнена в Лаборатории ядерных проблем ОИЯИ.

1. INTRODUCTION

The interest to multiple production processes noticeably falls down during last decades and this trend is understandable. Indeed, it is hard to expect a new physics if (a) the processes are too complicated because of a large number of involved degrees of freedom and (b) there is not quantitative hadrons theory to describe the nonperturbative effect of color charge confinement.

It may be surprising at first glance that the asymptotically high multiplicity (AHM) processes are simple at least from theoretical point of view [1][2]. Nevertheless this is so and

---

[1] Permanent address: Inst. of Physics, Tbilisi, Georgia

[2] The AHM triggering problem will not be considered. It will be considered in subsequent paper, see also [2].

our aim is to demonstrate this suggestion. This follows from expectation that the fluctuations (quantum as well) are small considering AHM final states creation[3].

We wish to note firstly that the AHM final states are equilibrium since the corresponding entropy reach a maximum in the AHM region [3]. Then a comparatively small number of simplest parameters should be needed for AHM states description because of the correlations relaxation principle of Bogoliubov[4].

Besides, the AHM processes may become hard and, therefore, we may neglect (with exponential accuracy) the background low-p_t nonperturbative channel of hadrons production. Intuitively this suggestion is evident noting that in all soft Regge-like theories, with interaction radii of hadrons $\sim \sqrt{\ln s}$, one cannot 'stir' in the disk of area $\sim \ln s$ arbitrary number of partons, since the high-p_t cutoff. Then the Regge-like theories are unable to describe the multiplicities $n > \ln^2 s$, if each parton in the disk is a source of $\sim \ln s$ hadrons. At high energies the AHM domain is sufficiently wide ($\ln^2 s << n_{\max} \sim \sqrt{s}$) and, therefore, should be 'occupied' by hard processes [1]. Indeed, the mean transfer momentum of created particle grows with n_c, see [4].

So, the interest to AHM processes seems evident, since: (a) being hard, the experimental investigation of them may help to clear up the structure of fundamental Lagrangian, and (b) the theoretical predictions in this field are more or less clear in the asymptotically free theories.

It seems constructive to start investigation of hadron dynamics from AHM domain and, experienced in this field, go to the moderate multiplicities. The to-day experimental status of AHM is following. There is experimental data at TeVatron energies up to $n_c \approx 5\bar{n}_c(s)$ [4]. The cross section $\sigma_{n_c} \approx 10^{-5}\sigma_{\text{tot}}$ at this values of charged particles multiplicity n_c. The events with higher multiplicity are unknown, if the odd cosmic data is not taken into account. The main experimental problem to observe AHM is smallness of corresponding cross sections and impossibility to formulate experimentally the 'naive' trigger tagging the AHM events by charged particles multiplicity[5]. We think that this question is very important since otherwise the AHM problem stay pure academic.

In Sec.2 we will give the physical interpretation of possible asymptotics over n. In Sec.3 the hard Pomerons contribution in AHM domain is discussed. In Sec.4 we will describe the QGP formation signal at AHM.

2. CLASSIFICATION OF ASYMPTOTICS OVER n

It is better to start from pure theoretical problem assuming that the incident total CM energy $E = \sqrt{s}$ is arbitrarily high and to consider asymptotics over the total multiplicity n, assuming nevertheless that $n << n_{\max} = \sqrt{s}/m$, where $m \simeq 0.2$ Gev is the characteristic

[3]The space density of colored constituents becomes large and 'cold' in the AHM domain.

[4]In this case, following the ergodic hypothesis, one may restrict oneself by event-by-event measurements, i.e. it is sufficient to have a small number of AHM events. This seems important from experimental point of view since the cross sections in the AHM domain are assumed extremely small.

[5]We suggest to reject tagging the event by the multiplicity noting that it is enough to have the 'cold' final state in the AHM domain [2]. Moreover, formulating the theory we would try to generalize ordinary inclusive approach [5].

hadron mass, to exclude the influence of phase space boundaries. Last one means that in the sum

$$\Xi_{\max}(z,s) = \sum_{n=1}^{n_{\max}} z^n \sigma_n(s)$$

we should choose the real positive z so small that upper boundary is not important and we can sum up to infinity:

$$\Xi(z,s) = \sum_{n=1}^{\infty} z^n \sigma_n(s). \tag{2.1}$$

This trick allows one to introduce classification of σ_n asymptotics counting the singularities of $\Xi(z,s)$ over z [1]. So, if z_c is the solution of equation:

$$n = z\frac{\partial}{\partial z}\ln \Xi(z,s), \tag{2.2}$$

then in the AHM region

$$\sigma_n \sim e^{-n \ln z_c(n,s)}. \tag{2.3}$$

To do further step we will use the connection with statistical physics [6]. By definition

$$\sigma_n(s) = \int d\omega_n(q)\delta(p_a + p_b - \sum_{i=1}^{n} q_i)|A_n|^2, \tag{2.4}$$

where A_n is the $a+b \to (n$ hadrons) transition amplitude and $d\omega_n(q)$ is the n particles phase space element. There is a well-known in the particle physics trick [7] as this $(3n)$-dimensional integrals may be calculated. For this purpose one should use the Fourier transformation of the energy-momentum conservation δ-function. Then, in the CM frame, if n is large,

$$\sigma_n(s) = \int \frac{d\beta}{2\pi} e^{\beta E}\rho_n(\beta), \tag{2.5}$$

where

$$\rho_n(\beta) = \int d\omega_n(q) \prod_{i=1}^{n} e^{-\beta\varepsilon_i}|A_n|^2, \tag{2.6}$$

and ε_i is the i-th particles energy.

Obviously this trick is used to avoid the constraints from the energy-momentum conservation δ-function. But it has more deep consequence. So, if we consider interacting particles a and b in the black-body environment, then we should use the occupation number $\bar{n}_{ext}$ instead of 'Boltzmann factor' $e^{-\beta\varepsilon_i}$. For bosons

$$\bar{n}_{ext}(\beta\varepsilon) = \{e^{\beta\varepsilon} - 1\}^{-1}. \tag{2.7}$$

In result, replacing $e^{-\beta\varepsilon_i}$ by $\bar{n}_{ext}$,

$$\Xi(\beta,z) = \sum_n z^n \rho_n(\beta) \tag{2.8}$$

would coincide *identically* with big partition function of relativistic statistical physics, where β is the inverse temperature $1/T$ and z is the activity: the chemical potential $\mu = T \ln z$ [8].

We may use this S-matrix interpretation of statistical physics and consider $\Xi(z,s)$ as the energy representation of the partition function. Then, following Lee and Yang [9], $\Xi(z,s)$ should be regular function of z, for practically arbitrary interaction potentials, in the interior of unite circle. This means, using estimation (2.3), that

$$\sigma_n(s) < O(1/n), \tag{2.9}$$

i.e., $\sigma_n(s)$ should decrease faster than any power of $1/n$.

First singularity may locate at $z = 1$. It is evident from definition (2.1) that $\Xi(z,s)$ would be singular at $z = 1$ iff

$$\sigma_n(s) > O(e^{-n}), \tag{2.10}$$

i.e., in this case $\sigma_n(s)$ should decrease slower than any power of e^{-n}. It follows from estimation (2.3), in this case $z_c(n,s)$ should be the decreasing function of n. Note that such solution is, at first glance, impossible. Indeed, by definition (2.1), $\Xi(z,s)$ should be increasing function of z since all σ_n are positive. Then the solution of Eq.(2.2) should be increasing function of n. But, nevertheless, such possibility exists.

Remember for this purpose connection of z with chemical potential, $z_c(n,s)$ defines the work needed for creation of additional particle. So, $z_c(n,s)$ may be the decreasing function of n iff the vacuum is unstable and the transition from false, free from colorless particles (or being chiral invariant, etc.), vacuum to the true one means colorless particles (or of the chiral-invariance broken states, etc.) creation. Just this case corresponds to the first order phase transition [9, 10].

This phenomenon describes expansion of the domain of new phase with accelerating expansion of the new phase domains boundary, if the radius of domain is larger than some critical value [11]. So, $z_c(n,s)$ should decrease with n since z is conjugate to physical particles number in the domain of new phase.

The following singularity in the equilibrium statistics may locate at $z = \infty$ only. This is the general conclusion and means, as follows from (2.3), that

$$\sigma_n(s) < O(e^{-n}). \tag{2.11}$$

In this case $\sigma_n(s)$ should fall down faster than any power of e^{-n}. Note, investigation of the Regge-like theories gives just this prediction [12].

But considering the process of particles creation it is too hard to restrict oneself by equilibrium statistics. The final state may be equilibrium, as is expected in the AHM domain, but generally we consider the process of incident (kinetic) energy dissipation into particles mass. At very high energies having the AHM final state we investigate the process of highly nonequilibrium states relaxation into equilibrium one.

Such processes have interesting property readily seen in the following well-known model. So, at the very beginning of this century couple P. and T.Euhrenfest had offered a model to visualize Boltzmann's interpretation of irreversibility phenomena in statistics [13]. The model is extremely simple and fruitful. It considers two boxes with $2N$ numerated balls. Choosing number $l = 1, 2, ..., 2N$ *randomly* one must take the ball with label l from one box and put it to another one. Starting from the highly 'nonequilibrium' state with all balls in one

box it is seen a tendency to equalization of balls number in the boxes. So, there is seen irreversible flow toward preferable (equilibrium) state. One can hope that this model reflects a physical reality of nonequilibrium processes with initial state very far from equilibrium. A theory of such processes with (nonequilibrium) flow toward a state with maximal entropy should be sufficiently simple to give definite theoretical predictions since there is not statistical fluctuation of this flaw.

Following this model one can expect total dissipation of incident energy into particle masses. In this case the mean multiplicity $\bar{n}$ should be $\simeq n_{\max}$ [3]. But it is well known that experimentally $\bar{n} << n_{\max}$. Explanation of this phenomena is hidden in the constraints connected with the conservation laws of Yang-Mills field theory. It is noticeable also that this constraints are not so rigid as in integrable systems, where there is no thermalization [14]. In the AHM domain we expect the free from above constraints dynamics. So, the AHM state may be the result of dissipation process governed by 'free' (from QCD constraints) irreversible flow.

The best candidates for such processes are stationary Markovian ones. They will be described by the so-called logistic equation [15] and lead to inverse binomial distribution with generating function

$$\Xi(z,s) = \sigma_{\text{tot}}(s)\left\{\frac{z_s(s)-1}{z_s(s)-z}\right\}^{\gamma}, \ \gamma > 0. \tag{2.12}$$

The normalization condition $\partial \ln \Xi(z,s)/\partial z|_{z=1} = \bar{n}_j(s)$ determines the singularity position:

$$z_s(s) = 1 + \gamma/\bar{n}_j(s). \tag{2.13}$$

Note, $z_s(s) \to 1$ at $s \to \infty$ since $\bar{n}_j(s)$ should be increasing function of s.

Mostly probable values of z tend to z_s from below with rising n:

$$z_c(n,s) \simeq z_s - \gamma/n = 1 + \gamma(\frac{1}{\bar{n}_j(s)} - \frac{1}{n}). \tag{2.14}$$

This means that the vacuum of corresponding field theory should be stable. It is evident that σ_n decrease in this case as the $O(e^{-n})$:

$$\sigma_n \sim e^{-\gamma n/\bar{n}_j}. \tag{2.15}$$

The singular solutions of (2.12) type arise in the field theory, when the s-channel cascades (jets) are described [16]. By definition $\Xi(z,s)$ coincide with total cross section at $z = 1$. Therefore, nearness of z_c to one defines the significance of corresponding processes. It follows from (2.14) that both s and n should be high enough to expect the jets creation. But the necessary condition is closeness to one of z_s, i.e., the high energies are necessary, and high n simplifies only their creation. Note the importance of jet creation processes in early Universe, when the energy density is extremely high.

Expressing the 'logistic grows law' the singular structure (2.12) leads to the following interesting consequence [15]. The energy conservation law shifts the singularity to the right. For instance, the singularity associated with two-jets creation is located at $z_c^{(2)}(s) = z_c(s/4) > z_c(s)$. Therefore, the multi-jet events will be suppressed with exponential accuracy in the AHM domain if the energy is high enough, since at 'low' energies even the exponential accuracy may be insufficient for such conclusion [1]. One may assume that there should be

the critical value of incident energy at which this phenomena may realized. So the AHM are able to 'reveal' the jet structure iff the energies are high enough. In this sense the AHM domain is equivalent of asymptotic energies.

Summarizing above estimations we may conclude that

$$O(e^{-n}) \leq \sigma_n < O(1/n), \tag{2.16}$$

i.e., the soft Regge-like channel of hadron creation is suppressed in the AHM region in the high energy events with exponential accuracy.

3. HARD POMERON

During last 50 years the contribution (Pomeron) which governs the s-asymptotics of the total cross section $\sigma_{\rm tot}(s)$ is to stay unsolved. The efforts in the pQCD frame show that the t-channel ladder diagrams from dressed gluons may be considered as the dynamical model of the Pomeron [17].

The BFKL Pomeron arises in result of summation, at least in the LLA, of ladder gluon diagrams in which the virtualities of space-like gluons rise to the middle of the ladder. To use the LLA these virtualities should be high enough. Noting that the 'cross-beams' (time-like gluons) of the ladder are the sources of jets it is natural that in the AHM domain the jet masses q_i^2 are large enough and one can apply the LLA.

Consideration of Pomeron as the t-channel localized object allows one to conclude that the multi-Pomeron contribution is $\sim 1/k!$ if k is the number of Pomerons. This becomes evident noting that in the t channel the distribution over k localized uncorrelated 'particles' should be Poissonian. This factorial damping should be taken into account in the AHM domain.

Following our above derived conclusion, number of 'cross-beams' (jets) should decrease with increasing n, and, therefore, in the AHM domain the BFKL Pomeron, with exponential accuracy, should degenerate into ladder with two 'cross-beams' only. The virtuality of time-like gluons becomes in this case $\sim \sqrt{s}$. So, the bare gluons are involved at high energies at the AHM. This soluton is in agreement with our general proposition that in the AHM domain the particles creation process should be stationary Markovian.

We conclude that the AHM processes gave unique possibility to understand as the BFKL Pomeron is built up. But there is the problem, connected with masslessness of gluons. So, the vertices of time-like gluons emission are singular at the $q_i^2 = 0$. It is the well-known low-x problem. In the BFKL Pomeron this singularity is canceled by attendant diagrams of the 'real' soft gluons emission. However, this mechanism should be destroyed when number of created particles (i.e., of gluons) is fixed. Note, the solution of this problem is unknown.

We hope to avoid this problem noting that the heavy jets creation dominates in the AHM domain. This idea reminds the way as the infrared problem is solved in the QED (The emission of photons with wave length much better than the dimension of measuring device is summed up to zero.) The quantitative realization of this possibility for QCD is in progress now.

4. QUARK GLUON PLASMA

There is a question: can we simulate in the terrestrial conditions the early Universe? The hot, dense, pure from colorless particles quark-gluon plasma (QGP) is the best candidate for investigation of this fundamental problem [18].

In our opinion [5] the plasma is a state of unbounded charges. The 'state' assumes presence of some parameters characterizing the collective of charges and the 'unbounded' assumes that the state is not locally, in some scale, neutral (we discuss the globally neutral plasma).

The ordinary QED plasma assumes that the mean energies of charged particles are sufficiently high (higher than the energy of particles acceptance), i.e., the QED plasma is 'hot'. The QCD plasma in opposite is not 'hot'(in corresponding energy scale) since the thermal motion moves apart the color charges. This leads to sufficient polarization and further 'boiling' of vacuum, with creation of $q\bar{q}$ pairs. So, the QCD plasma should be dense and at the same time 'cold' enough.

There is two principal possibilities to create such state. Mostly popular is QGP plasma formation in the heavy ion-ion collisions at high energies. It is believed that at the central (head-on) collisions one can observe the QGP in the CM central region of rapidities. But there are not in to-day situation the unambiguous (experimental) signals of QGP formation (number of the theoretical possibilities are discussed in literature).

Other possibility opens the AHM region: since in this region the hard channel of particles creation is favourable dynamically (at high energies), one can try to consider the collective of color charges on preconfinement stage as the plasma state. Because of energy-momentum conservation this state would be 'cold'. We should underline that possible cold QGP (CQGP) formation is just the dynamical, nonkinematical, effect: the estimation (2.16) means that the sufficient polarization of vacuum and its 'boiling' effects are insufficient, are frozen, at the AHM. So, considered CQGP remains relativistic. This solves the problem of unbounded charges formation[6].

But the question – may we consider the collective of colored charges created in the AHM events as the 'state' – remains open. To-day situation in theory is unable to give answer to this question (even in the QCD frame, this will be discussed). But we can show the experimentally controlled condition when the same parameters may be used to characterize this collective.

For instance, we may examine in what conditions the mean energy of colored particles may be considered as such parameter. Let us return to the definition (2.5) for this purpose. To calculate the integral over β we will use the stationary phase method. Mostly probable values of β are defined by equation of state:

$$E = \partial \ln \rho(\beta, z)/\partial\beta. \tag{4.17}$$

It is well known that this equation has positive real solution β_c. Then, as was noted above, β_c coincides with inverse temperature $1/T$ and this definition of T is obvious in the micro-canonical formalism of statistical physics.

---

[6]To amplify this effect it seems reasonable to create AHM in the ion-ion collisons

The parameter β_c is 'good', i.e., has a physical meaning, iff the fluctuations near it are Gaussian (It should be underlined that the value of fluctuations may be arbitrary, but the distribution should be Gaussian). This is so if, for instance,

$$\frac{\rho^{(3)}}{\rho} - 3\frac{\rho^{(2)}\rho^{(1)}}{\rho} + 2\frac{(\rho^{(1)})^3}{\rho} \approx 0, \tag{4.18}$$

where, for identical particles,

$$\rho^{(k)}(\beta_c, z) \equiv \frac{\partial^k \rho(\beta_c, z)}{\partial \beta_c^k} =$$

$$(-z\frac{\partial}{\partial z})^k \int d\omega_n(q) \prod_{i=1}^{k} \varepsilon(q_i) f_k(q_1, ..., q_k; \beta_c, z) \tag{4.19}$$

and $f_k(q_1, ..., q_k; \beta_c, z = 1)$ is the k-particle inclusive cross section. Therefore, the (4.18) condition requires smallness of energy correlation functions. It is the obvious in statistics energy correlations relaxation condition near the equilibrium. One can find easily the same condition for higher correlation functions.

This conditions establish the equilibrium, when knowledge of one parameter (β_c in considered case) is enough for whole systems description. The analogous conditions would arise if other parameters are considered. For instance, the (baryon, lepton, etc.) charge correlations relaxation condition means the 'chemical' equilibrium. The quantitative expression of this phenomena is smallness of corresponding correlation functions.

This conditions are controllable experimentally. But it is hard to expect that at finite values of n, where the cross sections are not too small, above derived conditions are hold, even in the AHM region. Later we will find more useable from experimental point of view conditions making more accurate analyses.

5. CONCLUSION

The AHM events offer interesting possibility of investigating the phase transition phenomena. Noting that the system has a tendency to become equilibrium in the AHM domain and noting that the Gibbs free energy is $\sim \ln \Xi$, we can compare the heat capacity in the hadrons and photons (or leptons) systems in the AHM domain. This will be the direct measurement of phase transition.

ACKNOWLEDGEMENT

The discussions of the inside of BFKL Pomeron with L.Lipatov and E.Kuraev, and of the mini-jets creation in the semi-hard processes with E.Levin was fruitful. The important for us modern experimental possibilities were discussed with Z.Krumshtein, V.Nikitin. The AHM PYTHIA simulation results of M.Gostkin were used also in our theoretical considerations. We are sincerely grateful to all of them. We would like to thank V.G.Kadyshevsky for the kind and interesting discussions.

References

1. The first attempt to formulate the phenomenology of AHM was given in: Manjavidze J., Sissakian A. — JINR Rap. Comm., 1988, 5[31]-88, p.5.

2. Manjavidze J., Sissakian A. — JINR Rap. Comm., 1988, 2[28]-88, p.13.

3. This idea was considered at the very beginning of multiple production theory of L.Landau and E.Fermi.

4. Alexopoulos T. et al. — Phys. Rev. Lett., 1988, v.60, p.1622; Lindsey C. — Fermilab-Conf-91/336.

5. Manjavidze J., Sissakian A. — JINR Rap. Comm., 1998, 2[28]-88, p.54.

6. Manjavidze J. — El. Part. & At. Nucl., , 1999, v.30, p.123.

7. E.g. Satz H. — Nuovo Cim., 1965, v.37, p.1407 and references cited in the textbook of E.Byckling and K.Kajantie, Particle Kinematics, John Wiley, Sons, London, 1973.

8. Actually this theory is identical to the so-called real-time finite temperature field theory: Schwinger J. — J. Math. Phys., 1964, v.A9, p.2363; Keldysh L. — JETP, 1964, v.20, p.1018. Further development one can find in the review papers, e.g.: Landsman N.P., wanWeert Ch.G. — Phys. Rep., 1987, v.145, p.141.

9. Yang C.N., Lee T.D. — Phys. Rev., 1952, v.87, p.404; J.S.Langer. — Ann. Phys., 1967, v.41, p.108.

10. Kac M., Uhlenbeck G.E., Hemmer P.C. — J. Math. Phys., 1963, v.4, p. 2.

11. Coleman S. — Whys in Subnuclear Physics, ed. by Zichichi, Ettore Majorana School, Erice, Italy, 1976; see also the paper of J.S.Langer in [9]

12. Manjavidze J. — El. Part. & At. Nucl., 1985, v.16, p.101.

13. Description and discussion of this model is given in: Probability and Related Topics in Physical Sciences, ed. by M.Kac, Interscience Publ., London, 1957.

14. Zakharov V. — JETP, 1973, v.65, p.219.

15. Such type of equation was arisen firstly in the populations grows theory: Volterra V. — Lecons sur la Theoreie Mathematique de la Lutte Pour la Vie, Paris, 1931.

16. Such structures was considered firstly in: Konishi K., Ukawa A., Veneziano G. — Phys. Lett., 1979, v.B80, p.259; Basseto A., Ciafaloni M., Marchesini G.. — Nucl. Phys., 1980, v.B163, p.4777.

17. Kuraev E.A., Lipatov L.N., Fadin V.S. — Sov. Phys. JETP, 1977, v.45, p.199; Balitski Ya.Ya., Lipatov L.N. — Sov. J. Nucl. Phys., 1978, v.28, p.822; Fadin V.S., Lipatov L.N., — Nucl. Phys., 1996, v.B477, p.767.

18. One can find description of the QGP to-day status and the ample list of references in the topical review of S.A.Bass, M.Gyulassy, H.Stocker, W.Greiner, hep-ph/9810281

19. The relativistic generalization of the Wigner functions approach was offered in the paper of Carrusers P., Zachariazen F. — Phys. Rev., 1986, v.D13, p.950; see also Carrusers P., Zachariazen F. — Rev. Mod. Phys., 1983, v.55, p.245.

Received on September 1, 1999.

УДК 539.12

TRIGGERING OF HIGH-MULTIPLICITY EVENTS USING CALORIMETRY

G.Chelkov, M.Gostkin, J.Manjavidze[1], *A.Sissakian, S.Tapprogge*[2]

The experimental investigation of asymptotically high multiplicity hadron reactions is discussed for the LHC, making use of calorimetry. The first investigation concerning the triggering of such events with calorimeter information only is described.

The investigation has been performed at the Laboratory of Nuclear Problems, JINR.

Триггирование событий с большой множественностью с использованием калориметрии

Г.Шелков и др.

Обсуждается экспериментальное исследование на LHC адронных реакций с асимптотически большой множественностью при использовании калориметрии. Описано первое исследование, касающееся триггирования таких событий с помощью только калориметрической информации.

Работа выполнена в Лаборатории ядерных проблем ОИЯИ.

1. INTRODUCTION

We believe now that the principle of elementary particle theory is known. It should be built on the basis of non-Abelian gauge theories, adding Lorentz covariantness and a renormalizability condition and, maybe, duality. There are only two fundamental questions: (A) the problem of mass hierarchies and (B) the problem of Grand Unification. Other questions, like confinement and so on, are more of a technical character.

An experiment may only give an answer to the above questions by searching for the (heavy) superparticles, for the 'desert', and for the vacuum structure (Higgs bosons, topological defects, and so on). It is useful to be able to separate experimentally background effects from multiparticle processes.

The asymptotically high multiplicity (AHM) processes with $n \gg \bar{n}(s)$, where the mean multiplicity $\bar{n}(s)$ introduces the natural scale for n, seem to be of interest just by this reason [1]. First of all, hadron processes become *hard* in the AHM domain. This means that

---

[1]Permanent address: Inst. of Physics, Tbilisi, Georgia

[2]EP Division, CERN, Geneva

during the process of AHM production nonperturbative effects are 'frozen' and perturbative QCD predictions are available. Note also the expected enhancement of heavy particles in such processes: the initial energy would be spent mostly on the creation of particle mass.

We have every reason to believe that AHM states are in equilibrium since the corresponding entropy reaches a maximum in the AHM region [3]. Therefore, secondly, the final states of AHM processes are close to *equilibrium* and a few parameters only are important for the description of such states. Indeed, the asymptotic estimation shows that $-\ln\{\sigma_n/\sigma_{\rm tot}\}/n = \mu(n) + O(1/n)$ in the AHM domain, where $\mu(n)$ is the chemical potential. Note, that the cold equilibrium state is the best arena for collective phenomena to occur.

AHM processes may also be used for the creation of a dense, practically pure, cold quark-gluon plasma (CQGP) [2]. To describe this state the collective parameters (temperature, chemical potential) would be sufficient enough. So we hope, that the observation of high-multiplicity processes will allow one to investigate the following topics [1]:

1. The creation of (super)heavy particles and gluon jets with extremely high $E_\perp$ (since the AHM processes are hard),

2. Collective phenomena in the colored system (since the final state of AHM is near the equilibrium). We want to emphasize that this information is unreachable in other type of experiments.

It is expected that at LHC energies the total mean multiplicity is $\bar{n} \sim 100$. At the same time, the maximal value of the multiplicity is $n_{\max} = \sqrt{s}/m \simeq 70\ 000$, where m is the characteristic hadron mass scale $m \sim 0.2$ GeV. So, the AHM domain includes events containing of the order of 10 000 particles in the final state.

Studies of AHM phenomena are at the very beginning and the aim of this paper is to discuss a possible way for an experimental selection of these events, which could be used as a trigger at LHC conditions. This question seems to be the most important since (i) the cross sections σ_n in the AHM domain are extremely small, i.e., $\sigma_n \ll 10^{-6}\sigma_{\rm tot}$ and it is very difficult to measure such small cross sections in the environment of high luminosity at the LHC for events without a clear signature (such as, e.g., a high $p_\perp$ lepton). Moreover, (ii) we wish to consider n as the *total* multiplicity, including neutral particles (by triggering on the charged particle multiplicity – which in itself presents a huge challenge in the environment of the LHC – we *might* suppress the creation of neutral particles in the AHM domain). A more detailed discussion on the physics of the AHM domain will be given in subsequent papers.

Our main idea is that in the AHM domain it is unimportant to know the strict value of the multiplicity. Therefore it may be sufficient to define n with certain, but controllable accuracy. For this purpose we want to try to use information coming from calorimetry only. We will show that a measurement of the total energy deposition in the calorimeter, (having a reasonable acceptance) allows one to fix the region of values $n \gg \bar{n}(s)$.

2. MONTE CARLO SIMULATION

A sample of 10^7 events for proton-proton collisions at $\sqrt{s} = 14$ TeV was generated with PYTHIA 5.7 [4]. Hard scattering (QCD high-$p_\perp$) processes for the initial parton states qq, qg and gg (PYTHIA subprocesses 11,12,13,28,53,68), and additionally low-$p_\perp$ production

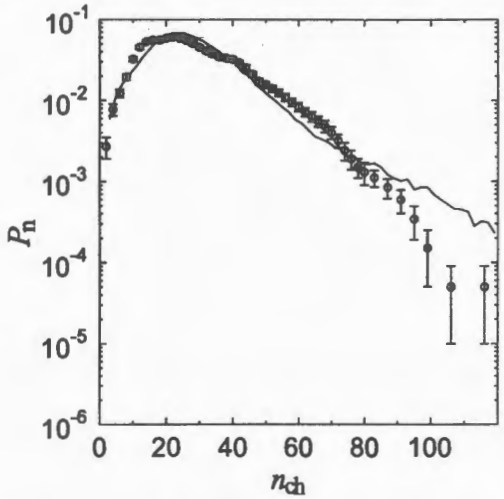

Fig. 1. Charged multiplicity distribution at 540 GeV [6], the solid line shows the prediction of the Monte Carlo calculation

(PYTHIA subprocess 95) were considered. In addition the framework of the Multiple-Interaction Model was used, with a variable impact parameter and an overlap of the hadronic matter being consistent with a double Gaussian matter distribution [5]. This model was chosen, since it is (at moderate multiplicities) in quite good agreement with the available experimental data [6] at 540 GeV and predicts a long tail in the AHM domain, as can be seen in Fig. 1. The latter provides large enough statistics for events with a very high multiplicty (the correctness of the cross section was not important at this stage).

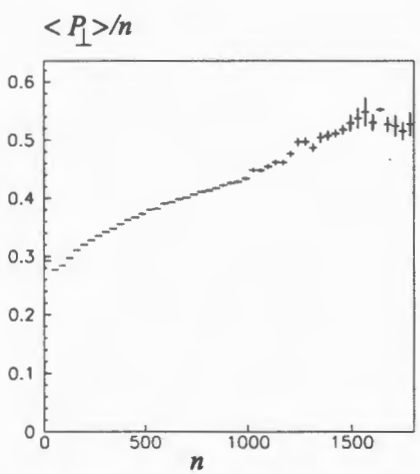

Fig. 2. Dependence of the average $< P_\perp > /n$ on the total multiplicity n

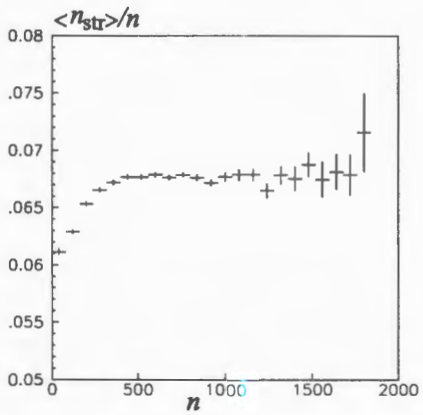

Fig. 3. Dependence of the strange particle fraction $< n_{str} > /n$ on the total multiplicity n

As mentioned above, we expect that for high energies and high multiplicities the particle creation processes would have a tendency to become hard [2]. Due to this, the mean transverse momentum of all particles and the mean strange particle multiplicity should rise with growing

total multiplicities. Figures 2 and 3 show the dependence of the average transverse momentum $\langle p_\perp \rangle / n$ per particle and of the yield of strange particles on the total multiplicity n as obtained from PYTHIA 5.7. One can see that the average transverse momentum and the yield of strange particles slightly grow with the total multiplicity in the model used.

Next we want to understand the effect of not being able to measure the particles themselves, but only to measure their energy deposition in a calorimeter. For this purpose, first a model of an ideal calorimeter was used. It is supposed to have a realistic angular acceptance with perfect energy resolution. In addition no lower cut-off on the momentum of the particles was required. In other words, all particles with pseudorapidities $\eta < 4.9$ (corresponding to the acceptance of the ATLAS calorimetry [7]) were considered as being detected.

Using this assumption, the total multiplicity (including neutral particles) distribution n was compared to the total energy deposition in the calorimeter, as shown in Fig. 4. A clear correlation between the two quantities is found. The mean value of the total multiplicity $\langle n \rangle$ is shown in Fig. 5 as a function of the energy deposition in the calorimeter E_{prime}. One can see that $\langle n \rangle$ increases with increasing E_{prime}.

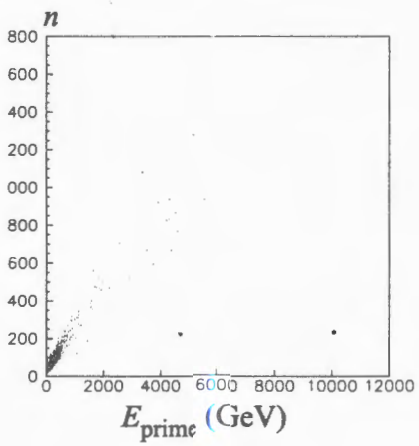

Fig. 4. Correlation between the multiplicity n and the total energy E_{prime} within $|\eta| < 4.9$

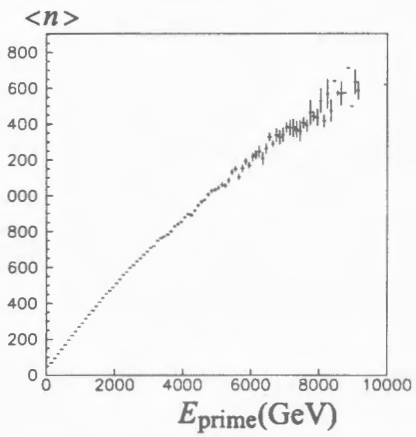

Fig. 5. Correlation between the average multiplicity $< n >$ and the total energy E_{prime} (for $|\eta| < 4.9$)

Finally, a few hundred events were simulated with the ATLSIM/DICE package [7], which contains a detailed simulation of the ATLAS detector response. This takes into account the effect of the magnetic solenoidal magnetic field on the detection of low momentum particles. In Fig. 6 one can see the same behavior for $\langle n \rangle = f(E_{\text{calo}})$, where E_{calo} is the energy deposited in the ATLAS calorimeters, as obtained from the ATLSIM/DICE simulation. Two fits of a linear dependence of $\langle n \rangle$ on E_{calo} are shown: the dotted line corresponds to the case of a 'real' ATLAS calorimeter; the solid line, to an ideal calorimeter with the same angular acceptance. The energy deposition in the case of the ATLAS calorimeter is about 20% smaller than for the ideal one.

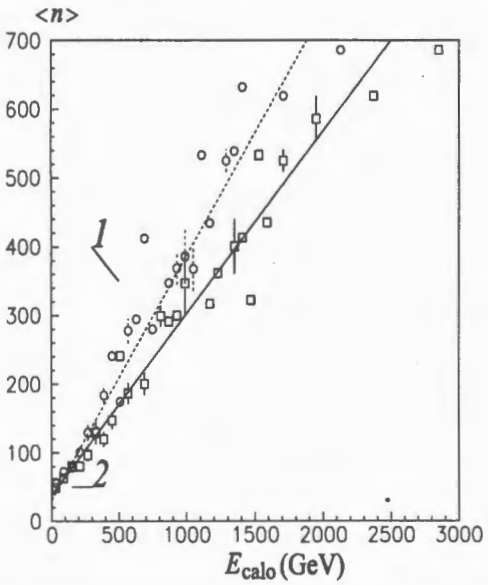

Fig. 6. Correlation between the average multiplicity $< n >$ and the total energy E_{calo} within $|\eta| < 4.9$. The circles are using the real calorimeter, and the dotted line is the corresponding fit. The squares are PYTHIA without detector simulation, the solid line is the fit to the latter points.

3. CONCLUSION

We conclude from this first study that *asymptotically high multiplicity* events can be triggered using the measurement of the total deposited energy in a calorimeter. This result is important since it opens the possibility to enlarge the experimental investigations in a domain where one may expect new physical phenomena. Further studies are needed to refine the selection criteria and on the other hand to quantify the knowledge on the value of the multiplicity from a calorimetric measurement (and to assess the capabilities of the tracking detectors to measure the charged component of the total multiplicity).

ACKNOWLEDGMENTS

We are grateful to the ATLAS collaboration who have taken interest in our work. We wish to thank S.Baranov for helpful advice concerning the use of ATLSIM and DICE.

References

1. Chelkov G., Manjavidze J., Sissakian A. — JINR Rap. Comm., 1999, 4[96]-99, p.35.
2. Manjavidze J., A.Sissakian — JINR Rapid Comm., 1998, 2[88]-98, p.51.
3. This idea was considered at the very beginning of multiple production theory of Landau L. and Fermi E.

4. Sjöstrand T. — Comput. Phys. Commun., 1994, v.82, p.74.

5. Sjöstrand T., van Zijl M. — Phys. Rev., 1987, v. D36, p.2019.

6. Alner G.J. et al. — UA5 Coll. — Phys. Rep., 1987, v.154, p.247.

7. ATLAS Collaboration, ATLAS Detector and Physics Performance TDR, vol. I, CERN/LHCC 99-14 (1999);
ATLAS Collaboration, ATLAS Detector and Physics Performance TDR, vol. II, CERN/LHCC 99-15 (1999).

Received on September 2, 1999.

УДК 621.384.633.6

ORBIT-3.0 — A COMPUTER CODE FOR SIMULATION AND CORRECTION OF THE CLOSED ORBIT AND FIRST TURN IN SYNCHROTRONS

D.Dinev[1]

A new computer program ORBIT-3.0 for simulation and correction of the closed orbit and first turn in synchrotrons is described. The program works under WINDOWS 95/98/NT and is a full object oriented application. It has an interactive interface, enhanced graphical capabilities and on-line printing. The original algorithms DINAM — for closed orbit correction and FTURN — for first turn steering are described as well.

The investigation has been performed at the Institute for Nuclear Research and Nuclear Energy, Bulgaria.

ORBIT-3.0 — компьютерная программа для моделирования и коррекции замкнутой орбиты и первого оборота в синхротронах

Д.Динев

Описана компьютерная программа ORBIT-3.0 для моделирования и коррекции замкнутой орбиты и первого оборота в синхротронах. Программа работает под WINDOWS 95/98/NT и полным набором ориентированных приложений. Она представляет собой интерактивный интерфейс, дополненный графическими возможностями с он-лайн распечаткой. Также описаны первоначальные алгоритмы DINAM — для замкнутой орбиты и FTURN — для управления первым оборотом.

Работа выполнена в Институте ядерных исследований и ядерной энергии, Болгария.

1. INTRODUCTION

One of the major tacks of the optimum operation of a cyclic charged particle accelerator of synchrotron type is the control and the correction of the equilibrium closed orbit. Due to the errors in the dipole magnetic fields, random transversal displacements of the quadrupoles from the reference orbit, random tilts of the dipole magnets around the longitudinal axis, stray magnetic fields and ground movements the real closed orbit is distorted. The maximum

[1]Institute for Nuclear Research and Nuclear Energy, 72 Tzarigradsko chaussee, 1784, Bulgaria

deviations of the distorted orbit from the reference orbit may reach some ten millimetres. Such large deviations do not allow one to use effectively the accelerator aperture and destroy the optimum work of the injection and extraction systems. For these reasons synchrotrons have special magnetic systems for correcting the closed orbit.

Special orbit correction algorithms have been developed in order to set the proper strengths of the orbit correctors [1]. Each of these algorithms has its specific advantages and disadvantages.

One of the major tacks at the design time of any synchrotron is to assess the most probable mean orbit deviation and the orbit amplitude as well. Several approximate analytical estimations have been found [2], but the computer simulations still remain a safer approach. Knowing these estimations helps us to design an adequate orbit correcting system.

A special problem is the first turn steering.

During the assembling and initial tuning of the accelerator much bigger errors than the usual random field and alignment errors may occur. Sometimes they are caused by unpredictable mistakes and there are several such cases in the accelerator practice. In the presence of big linear errors the centre of charge trajectory does not follow any more the orbit and can have big deviations from it. Even more, the beam can hit somewhere the vacuum chamber not being able to make a complete turn around the machine. Another case is when the first turn doesn't close onto the second. Along with the launch errors during injection this may cause harmful coherent oscillations of the beam.

Many of the widespread computer codes created for general accelerator design — MAD [3], DIMAD [4], PETROC [5] and others — possess features for calculating the closed orbit under the influence of random errors and incorporate one of the orbit correction methods. However these programs have no build-in capability for making statistics both of orbit and of its correction over an ensemble of some hundred or some thousand random machines. Such feature is very helpful during the accelerator design.

It is also advisable to compare different correction algorithms by means of computer simulations before to make your choice in favour of one of them.

In addition the problem of first turn threading and closing lies beyond the scope of interest of the above-mentioned general purpose programs. Specialized computer codes have been developed for first turn steering [6,7].

Last but not least is the old fashion interface of all these programs. Designed as a rule in the 70s for the monstrous old computers and gradually improved in the time these general accelerator design programs are not interactive and have limited graphical capabilities (usually a sort of off-line graphics). They are far from the now standard Windows-type interface as well.

In 1991, I developed the computer code ORBIT-2.0, especially intended for closed orbit simulation and correction. The computer code was created for the needs of the COler SYnchrotron COSY-Julich [7]. ORBIT-2.0 was written in C and runs on PCs under MS DOS. This is a menu driven program with enhanced graphical capabilities. A UNIX version with off-line graphics and printing was developed as well. Now a full MS WINDOWS 95/98/NT computer code ORBIT-3.0 for simulation and correction of both closed orbit and first turn is available.

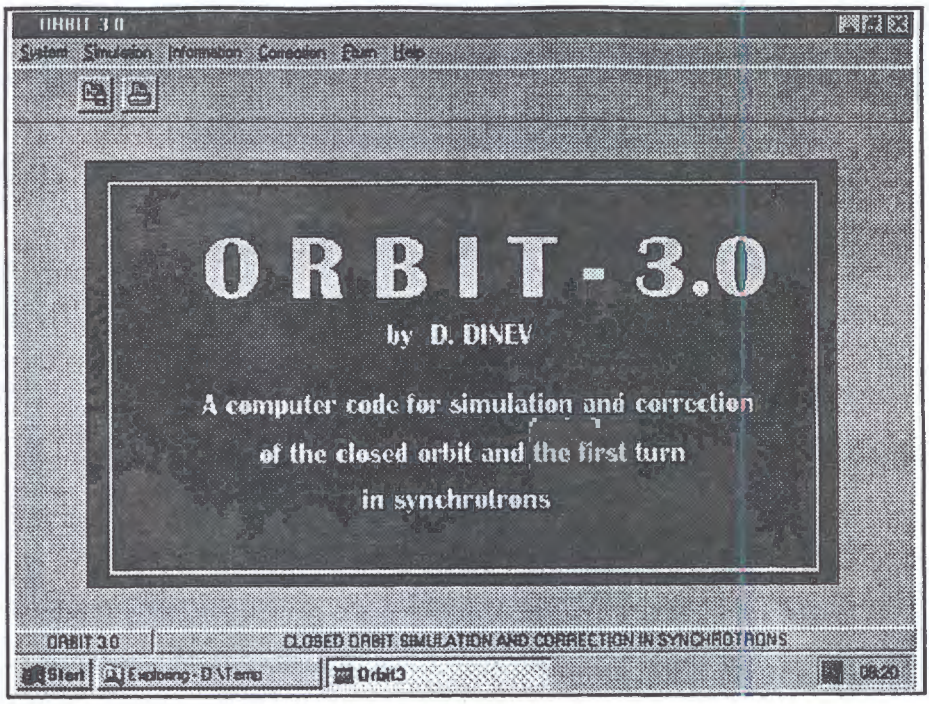

Fig. 1. Computer code ORBIT-3.0

2. COMPUTER CODE ORBIT-3.0

2.1. General Description. The computer code ORBIT-3.0 is a full MS WINDOWS 95/98/NT application. It is written in C++ and uses all the advantages of the object oriented programming. As a windows application ORBIT-3.0 has access to the big collection of WINDOWS resources and especially on-line printing , of both text and graphics on all the installed printers. The program has an interactive interface and enhanced graphical capabilities.

2.2. Main Options. The ORBIT-3.0 options are grouped in four groups: closed orbit simulation and statistics; processing of real orbit measurement data in order to produce some kind of additional information; correction of the measured or simulated orbits; first turn steering (Fig.1).

2.3. Orbit Simulation. As is well known the equation of transverse particle motion under linear perturbations can be put in the form of a forced oscillation equation by proper choice of the variables [1]. The 2π-periodic solution, i.e., the closed orbit can be represented by the formula:

$$\eta = \frac{Q}{2\sin \pi Q} \int_{\phi}^{\phi+2\pi} f(t) \cos Q(\phi + \pi - t) dt. \qquad (1)$$

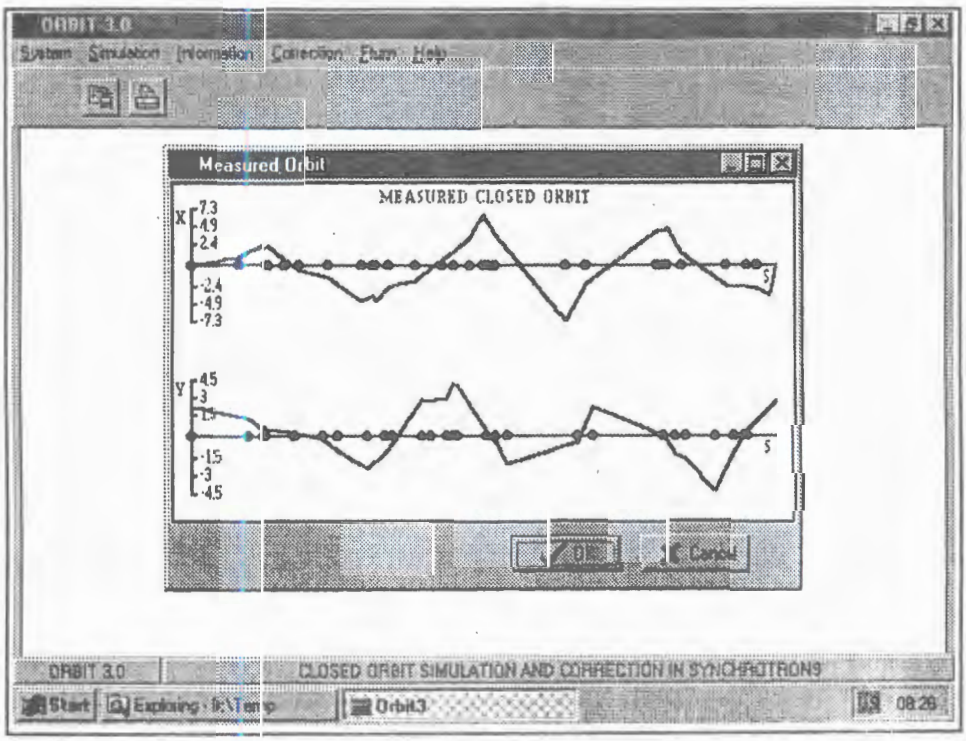

Fig. 2. Graphical representation of the closed orbet

In (1) $f(t)$ is a function which describes the linear perturbations, Q is the tune and:

$$\eta = \frac{x}{\sqrt{\beta(s)}}, \quad \phi = \int_0^s \frac{ds}{Q\beta(s)}, \tag{2}$$

$\beta(s)$ being the Twiss's amplitude function, x — the transverse and s — the longitudinal coordinates. It is very important to obtain a realistic predictions about the closed orbit behaviour in the future machine during the design period. The aperture of the vacuum chamber and the maximum strengths of the orbit correctors are determined on the base of the rms and maximum orbit deviations from the reference orbit. Knowing from the magnet measurements the dipole field errors $\Delta B/B$ and from the geodesy the expected transverse misalignments Δx and Δz and tilts $\Delta\theta$ of the elements one can calculate the statistical characteristics of the future orbit. In ORBIT-3.0 this is done either analytically applying the formulae obtained in [2] or by means of computer simulations. In [2] the variance of the maximum orbit amplitude is calculated taking into account only the major four orbit harmonics. ORBIT-3.0 calculates the value of the maximum orbit amplitude that will not be exceeded by 98% probability, the mean and the maximum rms deviations, and the rms orbit amplitude.

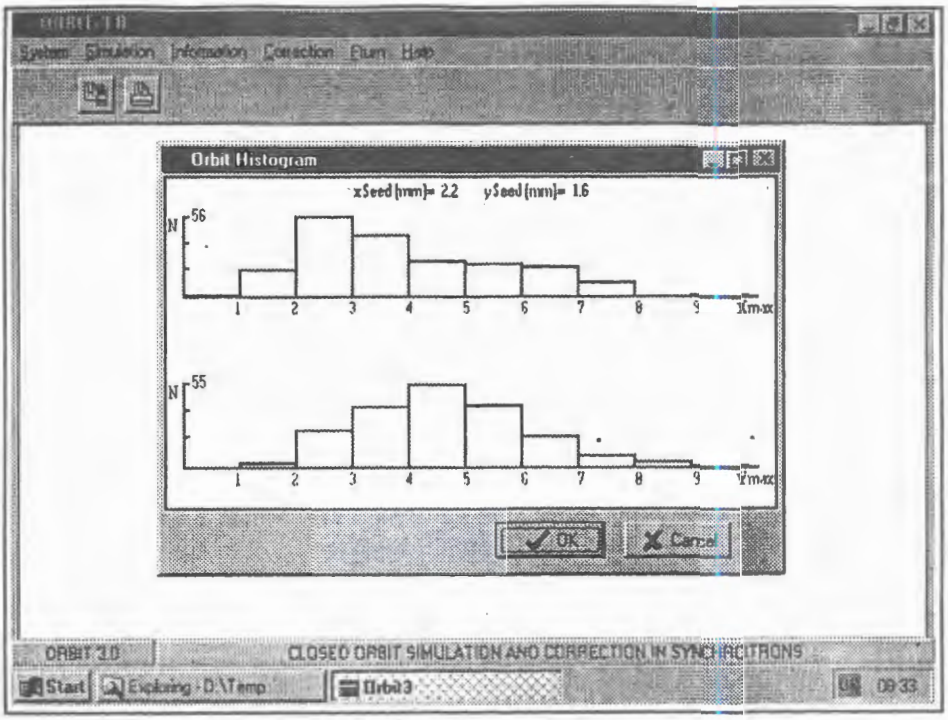

Fig. 3. Histograms of the simulated closed orbit

Another approach used for making orbit statistics is the simulation. An ensemble of identical machines with errors generated by a random number generator with Gaussian distribution is investigated. Closed orbits in each machine are represented either by tables of orbit deviations in beam position monitors (BPM) and structure elements or graphically (Fig.2). The results of orbit statistics are shown as histograms of maximum orbit amplitude distribution over the ensemble (Fig.3).

The Fourier spectrum of the simulated orbit is calculated through the well-known relation between harmonics of the perturbations f_k, g_k and orbit u_k, v_k:

$$u_0 = v_0, \quad u_k = \left(\frac{Q^2}{Q^2 - k^2}\right) f_k, \quad v_k = \left(\frac{Q^2}{Q^2 - k^2}\right) g_k. \tag{3}$$

2.4. Orbit Information. This group of options embraces features for processing the data of real orbit measurements in order to produce some sort of additional information.

First of all it is possible for the picture of the measured orbit along the machine circumference to be shown on the screen and printed in a selected printer.

A task that one frequently faces in the practice is to calculate the orbit deviations between BPMs. ORBIT-3.0 offers two possibilities. In local interpolation mode the orbit deviations in some number of points along the circumference are calculated applying several interpolation

methods. In general interpolation mode, the orbit in all the structure elements of the machine is restored on the base of BPMs measurements.

Finally the Fourier spectrum of the measured orbit could be calculated trough FFT and shown on the screen.

2.5. Orbit Correction. ORBIT-3.0 includes six algorithms for orbit correction: harmonic correction, beam-bump, least-squares (LSQ), singular value decomposition (SVD), Bacconier's method and DINAM. More information about these and other correction methods can be found in the review paper [1].

Harmonic correction is realised with the opportunity to set individual weights for each harmonic.

Beam-bump correction is coded for the case of arbitrary deployed correctors and monitors.

LSQ correction uses either LU matrix decomposition or Gauss-Jordan elimination methods for response matrix inversion.

SVD correction makes use of the singular value decomposition of the response matrix A:

$$A = UWV^T, \tag{4}$$

where U and V are unitary matrix and W is the diagonal matrix of the singular values w_i [9].

Obtaining the above decomposition of the response matrix, the vector of the corrections $\vec{\delta}$ is calculated through:

$$\vec{\delta} = -V[\mathrm{diag}\,(1/w_i)]U^T\vec{\eta}, \tag{5}$$

$\vec{\eta}$ being the vector of orbit deviations in BPMs. It should be emphasised that in case of some w_i, s equal to zero or very small (singular or ilconditioned response matrix), the corresponding diagonal elements $(1/w_i)$ in (5) must be replaced by zero $(\infty \to 0!)$.

In Bacconier's correction method the goal function is:

$$q = \gamma \sum_{n=1}^{N} \eta_i^2 + (1-\gamma) \sum_{j=1}^{K} \delta_j^2 \Rightarrow Min, \tag{6}$$

where η_i are the orbit deviations in BPMs, δ_j are the corrector strengths and γ is a parameter, $0 < \gamma < 1$.

As (6) reads, both the orbit deviations in BPMs and the strengths of the correctors are restricted thus reducing the influence of the remaining uncorrected higher harmonics of the correction.

DINAM is an original algorithm for orbit correction developed by the author and it will be described wider in the next chapter.

2.6. First Turn Steering. As we have mentioned in the introduction the first turn correction is a separate problem which frequently arises during the machine commitioning.

First of all we should thread the beam making it to perform a full turn around the accelerator. Having corrected the centre of charge trajectory so that the beam goes entire turn around the ring we should close this trajectory, i.e., make the second turn to coincide with the first one.

ORBIT-3.0 includes options for both first turn threading and first turn closing. The algorithm applied for this in ORBIT-3.0 will be described in the last chapter of this paper.

3. THE DINAM CORRECTION ALGORITHM

While the other orbit correction algorithms, described in detail in [1], strive to compensate the orbit deviations only in the points where BPMs are situated, the DINAM algorithm corrects the orbit over the whole accelerator ring. For that reason the criterion of correction quality is defined as the functional $q = (1/2\pi) \int_0^{2\pi} \eta^2(\phi) d\phi$ [10], where η is the orbit and ϕ is machine azimuth.

As the orbit $\eta(\phi)$ is a random function of the azimuth we should improve this criterion by taking the mathematical expectation of the functional:

$$q = M[(\frac{1}{2\pi} \int_0^{2\pi} \eta^2(\phi) d\phi. \tag{7}$$

With this choice of the correction quality we exclude the cases when the corrected orbit has approximately zero deviations in BPMs and relatively big deviations in between.

It is shown that the quality criterion can be put in the following form [10]:

$$q = \frac{1}{N} \sum_{i=1}^{N} \eta_i^2 + \frac{1}{2} \sum_{p=1}^{N} \sum_{q=1}^{K} A_{pq} \eta_p \delta_q + \frac{1}{2} \sum_{q=1} K \sum_{r=1}^{K} B_{qr} \delta_q \delta_r, \tag{8}$$

where η is the orbit, η is the corrector strength, N is number of BPMs and K is the number of orbit correctors. The coefficients A_{pq} and B_{qr} in (8) describe the optical parameters of the correction system and depend on ϕ_p, the azimuths of the BPMs and ϕ_q, ϕ_r, the azimuths of the correctors:

$$A_{pq} = \frac{2}{N} \left(c_0 + 2 \sum_{k=1}^{n/2-1} c_k \cos k(\phi_p - \phi_q) + c_{N/2} \cos \frac{N}{2} \phi_p \cos \frac{N}{2} \phi_q \right), \tag{9}$$

$$B_{qr} = \frac{c_0^2}{2} + \sum_{k=1}^{\infty} c_k^2 \cos k(\phi_q - \phi_r), \tag{10}$$

where:

$$c_k = \frac{2 \sin \pi Q}{\pi^2 (Q^2 - k^2)}. \tag{11}$$

The strengths of the orbit correctors are determined by the condition of minimum of q to occur. This leads to the following matrix equation for the correction vector $\vec{\delta}$:

$$\vec{\delta} = R\eta. \tag{12}$$

The matrix

$$R = -\frac{1}{2} A^{-1} B^T, \tag{13}$$

where $A = \{A_{pq}\}$ and $B = \{B_{pq}\}$.

The matrix depends only on the azimuths of the BPMs and of the correctors and for the given accelerator can be calculated prior to the correction.

Figure 4 shows an example of DINAM orbit correction.

The DINAM correction algorithm is relatively fast. It works reliably. It was used in the COSY-Julich and JINR-Nuclotron synchrotrons.

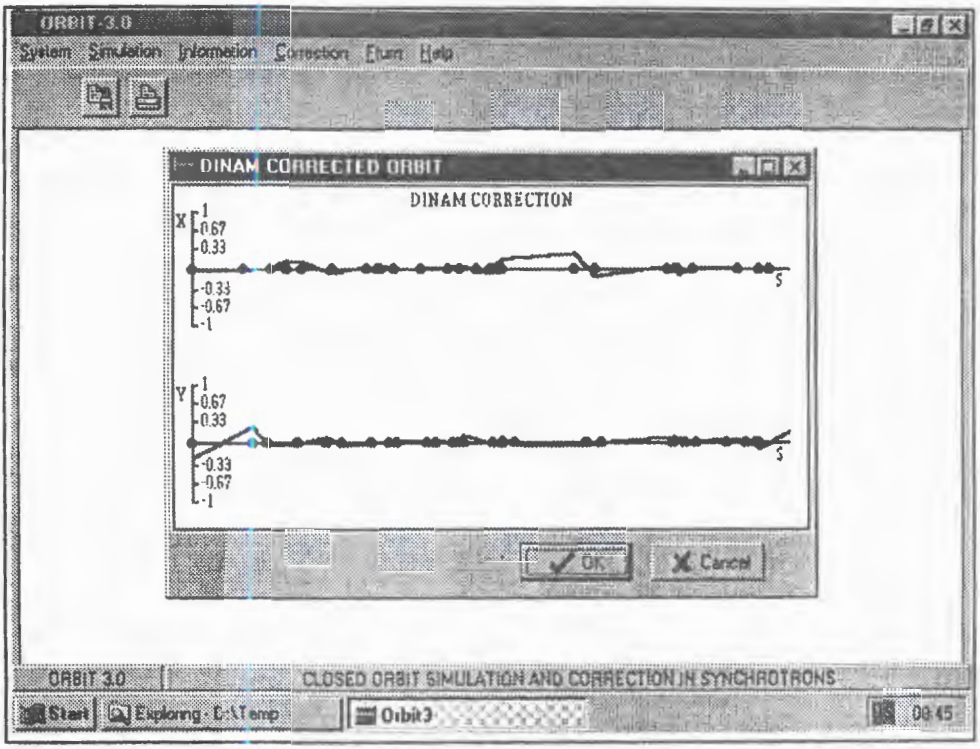

Fig. 4. DINAM closed orbit correction

4. FIRST TURN STEERING

In order to thread the beam entire turn around the accelerator ring and make the centre of charge trajectory to follow the injection orbit as close as possible an original first turn steering algorithm has been developed for ORBIT-3.0.

The algorithm uses the least squares approach but allows for constraints on the corrector kicks to be set.

The first turn correction is closely related to the beam line steering. In fact before closing the first turn onto the second the magnetic structure of a circular accelerator can be look at as a beam line. The BPMs «see» only those correctors which are deployed in front of them.

Applying the superposition principle one can write for the orbit deviation produced by the correctors in the i-th BPM:

$$\eta_i = \sum_{j=1}^{k} a_{ij}\epsilon_j^*, \tag{14}$$

where:

$$a_{ij} = \sin Q(\phi_i^{BPM} - \phi_j^C)e(\phi_i^{BPM} - \phi_j^C), \tag{15}$$

k being the number of used correctors and e — the Heaviside step function

$$\epsilon^* = \sqrt{\beta^C}\epsilon, \tag{16}$$

ϵ being the corrector kick.

Our algorithm follows the least squares approach.

In practice very often the available corrector strengths are not big enough for the exact correction to be realized. For that reason we have added parameter constraints to our algorithm. We used the penalty function method for that.

The goal function chosen is:

$$\Psi(\epsilon_j^*) = \sum_{i=1}^{n} \left[\eta_i^{BPM} - \eta_i^{des} + \sum_{j=1}^{k} a_{ij}\epsilon_i^* \right]^2 \Rightarrow min. \tag{17}$$

In (17) η_i^{des} denotes the desired centre of charge trajectory; n and k are the current numbers of used monitors and correctors. In the case when we have lost the beam before a full turn to be carried out the current number of used monitors n is less than the total number of monitors and the current number of switched on correctors k is less than the total number of available correctors K.

We should look for the minimum of (17) to occur under the following constrains on the corrector kicks:

$$|\epsilon_j| < \Delta, \quad j = 1, ..., k. \tag{18}$$

Thus we face a constrained optimization problem [11].

In order to solve this problem we apply the penalty function method. According to this method we reduce the constrained optimization problem to a series of unconstrained problems by adding to the goal function (17) the so-called penalty function $\alpha(\epsilon^*)$:

$$\Psi(\epsilon_j^*, \mu_k) = \Psi(\epsilon_j^*) + \mu_k \alpha(\epsilon_j^*) \Rightarrow Min, \tag{19}$$

where $\mu_k > 0$, $k = 1, 2, 3...$ are parameters and:

$$\lim_{k \to \infty} \mu_k = \infty. \tag{20}$$

The penalty function $\alpha(\epsilon^*)$ must «punish» the function $\Psi(\epsilon^*)$ if the constraints (18) are broken and in ORBIT-3.O we have chosen that:

$$\alpha(\epsilon_j^*) = \sum_{j=1}^{k} \max(0, \epsilon_j^{*2} - \Delta_j^2), \tag{21}$$

$$\Delta_j = \Delta\sqrt{\beta_j^C}. \tag{22}$$

Let ϵ_{jk}^*, $k = 1, 2, 3, ...$ be the consecutive points of minimum of $\Psi'(\epsilon_j^*, \mu_k)$. It can be proved [11] that:

$$\lim_{k \to \infty} \epsilon_{ij}^* = \epsilon_{j\,\mathrm{opt}}^* \tag{23}$$

and:

$$\lim_{k\to\infty}[\min \Psi\prime(\epsilon_j^*, \mu_k)] = \Psi(\epsilon_{j\,\mathrm{opt}}^*), \tag{24}$$

where $\epsilon_{j\,\mathrm{opt}}^*$ be the minimum of the goal function (17) under the constraints (18). After threading the beam entire turn around the accelerator we should ensure that the beam closes itself , i.e., that the second (and the following turns) coincide with the first turn. To perform the closing we need information about the first and second turn deviations in the first two BPMs. This information can be provided by these monitors if they work in a single turn mode. The beam closing in ORBIT-3.0 is achieved by appropriate tuning of the last two correctors in the ring.

References

1. Dinev D — Closed Orbit Correction in Synchrotrons. Physics of Particles and Nuclei, 1997, v.28, No.4, pp.1013—1060.

2. Gluckstern R. — Particle Accelerators, 1978, v.8, p.203.

3. Iselin F.C., Grote H. — The MAD Program — User's Reference Manual. Version 8.10. CERN No. SL 90 — 13, 1993.

4. Servranckx R., Brown K., Schachinger L., Douglas D. — User's Guide to the Program DIMAD. SLAC Report No. 285 UC — 28, 1985.

5. Guignard G., Marty Y. — CERN, Preprint No. LEP — TH/83 — 50, 1983.

6. Raya R., Rusell A., Aukenbrandt C. — Nuclear Instruments and Methods, 1989, v.A242, p.15.

7. Paxson V., Peggs S., Schachinger L. — Interactive First Turn and Global Orbit Correction. First European Particle Accelerators Conference EPAC—88, Rome, 1988, p.824.

8. Maier R.. Status of COSY. — Fourth European Particle Accelerators Conference EPAC—94, London, 1994.

9. Chung Y., Decker G., Evans K. — Proceedings of IEEE Particle Accelerators Conference, Washington, 1993.

10. Dietrich J., Dinev D., Martin S., Wagner R. — Simulation and Correction of the Closed Orbit in the Cooler Synchrotron COSY — Julich. Third European Particle Accelerators Conference EPAC—92, Berlin, 1992.

11. Gill P. E., Murray W., Wainwright M. H. — Practical Optimization. Academic Press, New York, 1982.

Received on September 22, 1999.

УДК 539.1.08; 612.82; 681.322

ОПРЕДЕЛЕНИЕ ХАРАКТЕРИСТИК ПАМЯТИ

П.М.Гопыч[1]

На основе теории проверки статистических гипотез предложены модельное определение и компьютерный метод вычисления характеристик памяти (вероятностей свободного вспоминания, вспоминания с подсказкой, узнавания), определение и способ вычисления интенсивностей подсказок, используемых при тестировании памяти человека. Предложены модели активных и пассивных следов памяти и установлено соотношение между ними. Показано, что ячейку автоассоциативной памяти в виде короткой двухслойной искусственной нейронной сети с повреждениями (или без повреждений) можно использовать для модельного описания характеристик памяти испытуемых с частично поврежденным (или здоровым) мозгом.

Determination of Memory Performance

P.M.Gopych

Within the scope of testing statistical hypotheses theory a model definition and a computer method for model calculation of widely used in neuropsychology human memory performance (free recall, cued recall, and recognition probabilities), a model definition and a computer method for model calculation of intensities of cues used in experiments for testing human memory quality are proposed. Models for active and passive traces of memory and their relations are found. It was shown that autoassociative memory unit in the form of short two-layer artificial neural network with (or without) damages can be used for model description of memory performance in subjects with (or without) local brain lesions.

1. ВВЕДЕНИЕ

Важнейшей задачей современной нейробиологии является выявление механизмов кодирования информации в нейронных структурах мозга человека и животных. Из-за междисциплинарности проблемы существенные результаты при ее исследовании часто получают, используя методы смежных дисциплин: эвристического моделирования [1], матричного исчисления [2], термодинамики [3], теории информации [4].

[1]Харьковский государственный университет, Украина; e-mail: pmg@pmg.kharkov.com

В настоящей работе на основе статистической теории принятия решений — выбора гипотез (см., например, [5]) предложены модельное определение и способ компьютерного вычисления некоторых количественных характеристик памяти — одной из важнейших когнитивных функций мозга. На важность учета процессов принятия решений при описании функционирования памяти указывалось еще в [6]. Основой предлагаемых результатов стали экспериментальные данные [7] о характеристиках зрительной системы человека-оператора, идентифицирующего (распознающего) одиночные пики на случайном аддитивном фоне в линейчатых спектрах излучения (это один из основных типов первичных экспериментальных данных в современном естествознании), и метод [8] их полного количественного описания с использованием теории искусственных нейронных сетей (см., например, [9, 10]).

Для применения статистической теории принятия решений необходимо в явном виде определить статистические свойства исследуемого объекта. В рамках настоящей работы предполагаем, что сам элемент (ячейка) памяти задается детерминированно, а статистические свойства связанного с ним явления памяти обусловлены статистическими свойствами обрабатываемых им сигналов. Поэтому определим вначале простейшую нейросетевую модель ячейки памяти и модели обслуживающих ее сигналов.

2. ПОСТАНОВКА ЗАДАЧИ

Рассмотрим двухслойную искусственную нейронную сеть (ИНС) с одинаковым числом N входных и выходных нейронов, с синаптическими связями, когда каждый нейрон входного слоя связан со всеми нейронами выходного слоя, со ступенчатой ответной функцией нейронов и нулевым порогом их срабатывания. Полагаем, что модельные нейроны бинарные, т.е. их входные и выходные сигналы принимают только одно из двух дискретных значений: –1 или +1 (можно полагать, что это модельное представление нервных импульсов, поступающих на вход соответственно тормозных и возбуждающих синапсов живых нейронов).

Произвольный набор сигналов на входе (выходе) рассматриваемой ИНС будем записывать в виде векторов $\mathbf{X}$ в ортогональном пространстве размерности N, все компоненты (проекции) которых могут принимать значения только –1 или +1. Тогда совокупность входных сигналов сети — это ее входной вектор $\mathbf{X}_{\text{in}}$, а совокупность выходных сигналов сети — это ее выходной вектор $\mathbf{X}_{\text{out}}$. Поскольку $\mathbf{X}_{\text{in}}$, $\mathbf{X}_{\text{out}}$ являются бинарными векторами одинаковой размерности N, то описанная ИНС представляет собой ячейку автоассоциативной [2, 4] памяти емкостью N бит.

Пусть $\mathbf{X}_0$ — произвольный вектор, значения проекций которого несут запоминаемую рассматриваемой сетью (ячейкой автоассоциативной памяти) информацию. Будем называть $\mathbf{X}_0$ вектором-эталоном. Правило, определяющее элементы синаптической матрицы ИНС при запоминании ею эталонного вектора, выберем, следуя Хопфилду [3], в виде

$$w_{ij} = \mathbf{X}_{0i}\mathbf{X}_{0j}/N, \tag{1}$$

где $\mathbf{X}_{0i}$ — i-я компонента входного вектора (входной сигнал i-го нейрона входного слоя сети); $\mathbf{X}_{0j}$ — j-я компонента выходного вектора (выходной сигнал j-го нейрона выходного слоя сети). Таким образом, в (1) предполагаем, что $\mathbf{X}_{\text{in}} = \mathbf{X}_{\text{out}} = \mathbf{X}_0$. По

этой причине $\mathbf{X}_{0i} = \mathbf{X}_{0j}$ при $i = j$ (i — номер входного нейрона, j — номер выходного нейрона). Видно, что межнейронные связи w_{ij}, необходимые для запоминания сетью вектора $\mathbf{X}_0$, соотношением (1) определяются однозначно, т.е. детерминированно (здесь и далее множитель $1/N$ несущественен, поэтому в дальнейшем его опускаем).

ИНС с межнейронными связями (1), определяемыми запомненным эталонным вектором $\mathbf{X}_0$, будем называть обученной сетью и, следуя [8], будем рассматривать правило (1) вычисления w_{ij} совместно с определяемыми ниже правилами (2)–(3) преобразования компонент входного вектора как алгоритм распознавания вектора $\mathbf{X}_0$. Если после преобразования обученной сетью произвольного входного вектора $\mathbf{X}_{\text{in}}$ на ее выходе возникает вектор $\mathbf{X}_{\text{out}} = \mathbf{X}_0$, то считаем, что сеть идентифицировала (узнала) запомненный ею эталон $\mathbf{X}_0$.

Преобразование входного вектора $\mathbf{X}_{\text{in}}$ в выходной вектор $\mathbf{X}_{\text{out}}$ происходит по таким правилам (см. [3, 8]).

Вычисление входного сигнала для j-го нейрона выходного слоя сети:

$$H_j = \sum w_{ij} V_i + S_j, \tag{2}$$

где суммирование по $i = 1, \ldots N$; V_i — выходной сигнал i-го нейрона входного слоя сети; S_j — сторонний сигнал (здесь $S_j = 0$).

Вычисление выходного сигнала V_j j-го нейрона выходного слоя сети (j-й компоненты выходного вектора $\mathbf{X}_0$):

$$V_j = \begin{cases} +1, \text{если} & H_j > 0 \\ -1, \text{если} & H_j \le 0. \end{cases} \tag{3}$$

Полагая H_i равным i-й компоненте входного вектора $\mathbf{X}_{\text{in}}$, с помощью (3) находят и выходной сигнал V_i для i-го нейрона входного слоя сети.

Предполагаем, что распознаваемый вектор-эталон может быть подвержен случайным искажениям. Тогда для количественного описания этих искажений надо определить понятие шума и правило, определяющее, как этот шум может искажать эталон.

В рамках рассматриваемого подхода проекции всех векторов могут принимать значения только –1 или +1, поэтому определим случайный вектор, или "шум", $\mathbf{X}_s$ как вектор, значения компонент которого –1 или +1 распределены случайно и равновероятно. Определим также искаженный эталонный вектор $\mathbf{X}(d)$ как вектор $\mathbf{X}_0$, искаженный (со степенью искажения d) шумом $\mathbf{X}_s$:

$$\mathbf{X}_i(d) = \begin{cases} \mathbf{X}_{0i}, & \text{если} \quad u_i = 0 \\ \mathbf{X}_{0i}, & \text{если} \quad u_i = 1, \quad \text{sign}(\mathbf{X}_{0i}) = \text{sign}(\mathbf{X}_{si}) \\ \mathbf{X}_{si}, & \text{если} \quad u_i = 1, \quad \text{sign}(\mathbf{X}_{0i}) \neq \text{sign}(\mathbf{X}_{si}), \end{cases} \tag{4}$$

где $\mathbf{X}_i(d), \mathbf{X}_{0i}, \mathbf{X}_{si}$ — i-е проекции искаженного вектора-эталона, вектора-эталона и шумового вектора; $i = 1, \ldots N$; u_i — признаки, значения которых "0" или "1" выбираем случайно и равновероятно с соблюдением условия нормировки

$$d = \sum u_i / N. \tag{5}$$

Ясно, что $0 \le d \le 1$, $\mathbf{X}(0) = \mathbf{X}_0$, $\mathbf{X}(1) = \mathbf{X}_s$.

В силу правила (1) (см. также [3, 8]) при анализе сетью вектора $\mathbf{X}_0$ на ее выходе обязательно возникает тот же вектор $\mathbf{X}_0$, т.е. обученная сеть узнает запомненный ею вектор-эталон с вероятностью 1. При анализе сетью случайного вектора $\mathbf{X}_s$ (т.е. шума) запомненный ею эталон $\mathbf{X}_0$ может возникнуть на выходе обученной ИНС только случайно. Следовательно, вероятность α случайной интерпретации шума в качестве эталона есть $\alpha < 1$. При анализе сетью вектора $\mathbf{X}(d)$ реализуется промежуточная ситуация и на выходе обученной ИНС эталонный вектор $\mathbf{X}_0$ возникает с вероятностью $P(d)$, для которой, по названным причинам, имеем: $\alpha \le P(d) \le 1, \quad P(1) = \alpha, \quad P(0) = 1$.

Линейчатые спектры излучения (более общий случай — результат цифрового сканирования произвольных штриховых изображений) можно преобразовать в набор векторов с компонентами из положительных или отрицательных единиц без потери информации, существенной для распознавания в них образов нейросетевыми алгоритмами [8]. При таком преобразовании (по правилам из [8]) участки спектра с хорошо выраженным пиком преобразуются в эталонный вектор $\mathbf{X}_0$, участки спектра со слабо выраженным пиком — в искаженный эталонный вектор $\mathbf{X}(d)$, со степенью искажения d, зависящей от отношения сигнал/шум для этого пика, а участки спектра без пиков (фон) — в одну из случайных реализаций вектора $\mathbf{X}_s$. Таким образом, определенные выше вектор-эталон, искаженный вектор-эталон и вектор шума действительно реализуются при нейросетевом анализе широко распространенных реальных статистических данных и, более того, все возможные варианты искаженных эталонных векторов $\mathbf{X}(d)$ исчерпывают все возможные варианты входных векторов $\mathbf{X}_{\text{in}}$ (напомним, $\mathbf{X}_0$, $\mathbf{X}_s$ являются частными случаями $\mathbf{X}(\text{d})$). Следовательно, если далее вместо $\mathbf{X}_{\text{in}}$ всюду использовать $\mathbf{X}(d)$, то общности рассмотрения это не ограничивает.

3. РЕЗУЛЬТАТЫ И ОБСУЖДЕНИЕ

Алгоритм распознавания (1)–(3) анализирует входные данные статистического характера, поэтому интерпретируем его как некий статистический критерий проверки простых альтернативных гипотез [5, 8].

Положим, что нулевая гипотеза H_0 состоит в том, что анализируемый сетью входной вектор $\mathbf{X}_{\text{in}} = \mathbf{X}(d)$ есть случайный вектор $\mathbf{X}_s$. Тогда альтернативная гипотеза H_1 состоит в том, что $\mathbf{X}(d)$ есть эталонный вектор $\mathbf{X}_0$ (хотя и искаженный дискретным бинарным шумом $\mathbf{X}_s$).

Вероятность отвергнуть H_0 есть уровень значимости критерия α [5], так как согласно приведенному выше определению входной вектор $\mathbf{X}_s$ интерпретируется сетью как эталонный с вероятностью α. Случайный вектор $\mathbf{X}_s$ (т.е. шум) не содержит какой-либо информации об $\mathbf{X}_0$ и, следовательно, α есть для обученной сети вероятность "вспомнить" запомненный ею вектор-эталон без подсказки. Роль шумового вектора $\mathbf{X}_s$ состоит здесь только в том, что он инициирует это вспоминание. Таким образом, α есть в одно и то же время уровень значимости критерия, вероятность ошибки первого рода, условная вероятность ложного обнаружения (вероятность ложной тревоги) и вероятность вспомнить запомненную информацию без подсказки (вероятность свободного вспоминания из памяти).

Пусть вероятность отвергнуть H_1, когда она верна, есть β, т.е. β — это вероятность ошибки второго рода [5]. Вероятность принять гипотезу H_1 при этом же условии

есть мощность критерия $M = 1 - \beta$, причем $M = P(d)$, так как согласно приведенному выше определению при анализе входного вектора $\mathbf{X}(d)$ на выходе ИНС эталонный вектор $\mathbf{X}_0$ возникает с вероятностью $P(d)$. Искаженный эталонный вектор $\mathbf{X}(d)$ содержит некую информацию об $\mathbf{X}_0$ (тем большую, чем меньше d), и эта информация "напоминает" ИНС о запомненном ею эталонном векторе или, другими словами, служит "подсказкой" при вспоминании обученной сетью эталона $\mathbf{X}_0$. Следовательно, P есть вероятность вспоминания сетью эталона $\mathbf{X}_0$ при наличии подсказки. Интенсивность этой подсказки q определим как $q = 1 - d$. Это простейшее определение q, для которого выполняется двойное неравенство $0 \leq q \leq 1$ и $q(d)$ монотонно растет с уменьшением d во всем допустимом диапазоне значений $0 \leq d \leq 1$ (см. выше). Таким образом, $P(d)$ или $P(q) = P(1 - d)$ есть в одно и то же время мощность статистического критерия проверки гипотез, условная вероятность истинного обнаружения искаженного вектора-эталона и вероятность вспомнить находящуюся в памяти информацию при степени ее искажения d или при интенсивности подсказки q. $P(0)$ есть при таком рассмотрении вероятность узнавания запомненного в памяти эталона, $P(1)$ — вероятность его свободного вспоминания (здесь и далее для определенности полагаем $P = P(d)$).

Таким образом, обычно определяемые [11] в нейропсихологических опытах количественные характеристики качества памяти человека — узнавание, свободное вспоминание и вспоминание с подсказкой — приобретают в рамках изложенного подхода строгий количественный смысл. Строгий количественный смысл приобретает и обычно используемое [11] в таких опытах понятие подсказки. Следовательно, для произвольного элемента памяти, независимо от того, принадлежит он живому организму или машине, можно определить ("измерить") характеризующие его качество вероятности $P(0)$, $P(1)$ и $P(d)$ при $0 \leq d \leq 1$. Для этого надо тестировать память большим количеством запомненных в ней образов с различной степенью их искажения d. В [7] приведены результаты такого тестирования зрительной системы человека-оператора графическими изображениями коротких фрагментов линейчатых спектров с пиками и без пиков, в [8] приведены результаты такого же тестирования описанных выше ИНС при анализе ими таких же, как в [7], спектров, но в цифровой форме. Методика выполнения упомянутых тестов с помощью компьютерного моделирования подробно описана в [12].

Отметим, что описанная модель памяти предполагает органичное сосуществование двух форм количественного описания следов памяти: 1) в виде синаптической матрицы (1), моделирующей специфическое распределение силы межнейронных связей в области мозга, ответственной за хранение запомненной информации (пассивный след памяти), 2) в виде входных и выходных бинарных векторов, являющихся моделями совокупности нервных импульсов, поступающих на вход или возникающих на выходе той же области мозга (активный след памяти). Матрица синаптических связей (пассивный след памяти) — это модель собственно запоминания (хранения) информации, причем весьма надежного, так как часто даже наличие сильных повреждений обученной сети не исключает полного извлечения запомненной в ней информации (см. ниже). Бинарные векторы (активные следы памяти) моделируют все виды передачи и обработки запомненной информации. Причем тот факт, что эти векторы именно бинарные, означает, что вычисления (обработка информации) в нервных тканях животных и человека выполняются, согласно рассматриваемой модели, в двоичной арифметике.

На рисунке приведены результаты количественного исследования качества описанной выше элементарной ячейки автоассоциативной памяти с помощью векторов $\mathbf{X}(d)$, гене-

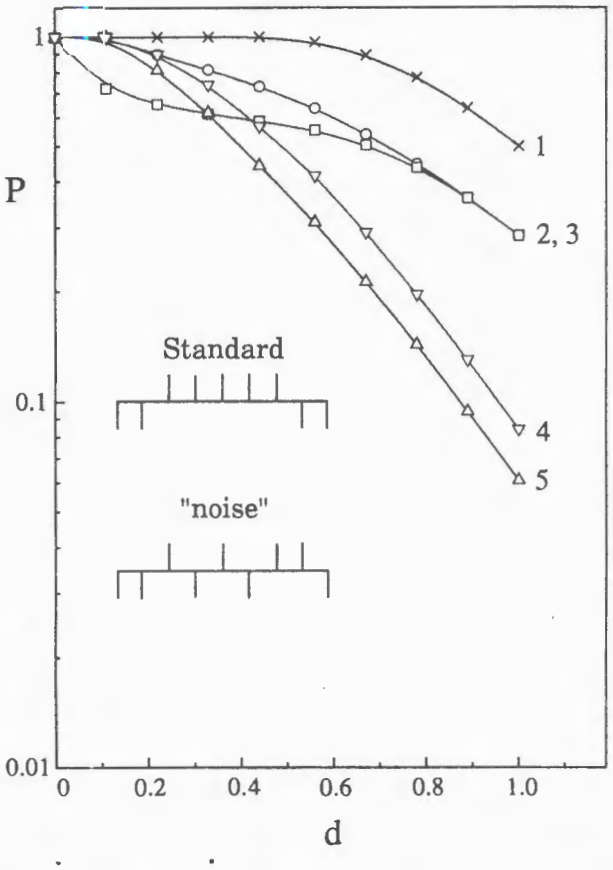

Вероятности $P(d)$ вспоминания (узнавания при $d = 0$) сетью с $N = 9$ запомненного ею эталонного вектора со степенью его искажения d; кривые — результат интерполяции вычисленных значений (различные значки). Слева схематически показаны эталонный (Standard) и пример случайного ("noise") векторов: черточки вверх и вниз означают соответственно компоненты этих векторов со значениями +1 и −1. Другие пояснения в тексте

рируемых по правилам (4), (5) при определенных (известных) значениях d для примера сети с $N = 9$. Такое N выбрано, чтобы облегчить сравнение приводимых и предшествующих [8] результатов и продемонстрировать, что даже при столь малом числе ассоциативных нейронов описанную ИНС можно использовать для количественного моделирования функциональных свойств живого мозга (в отличие от этого в [4] утверждается, что такое моделирование возможно лишь с использованием двухслойных нейронных сетей, содержащих не менее 10^6–10^7 ассоциативных элементов с числом синапсов на каждом из них $\sim 10^5$–10^6). На рисунке показаны зависимости $P(d)$ для неповрежденной (кривая *1*) и поврежденных (кривые 2–5) ИНС с $N = 9$. Здесь $P(d) = n_0(d)/n(d)$, где $n(d)$ — число разных генерируемых компьютером входных векторов $\mathbf{X}(d)$ со степенью искажения d вектора-эталона, $n_0(d)$ — число случаев, когда в результате анализа сетью входного вектора $\mathbf{X}(d)$ на ее выходе возникает эталонный вектор $\mathbf{X}_0$. Эталонный вектор $\mathbf{X}_0$ и пример

случайного вектора $\mathbf{X}_s$ показаны на рисунке внизу слева. При выборе вида $\mathbf{X}_0$ следовали работе [8]. Вероятности $P(d)$ вычисляли, анализируя все возможные варианты входных векторов $\mathbf{X}(d)$, так как при $N = 9$ $n(d)$ может быть полным числом таких вариантов (оно невелико): $n(d) = 2^m C_N^m$, где $d = m/N$; $m \leq N$ — число значений $u_i = 1$ в формуле (5). Так получаем точные значения $P(d)$; при больших N можно использовать метод многократных статистических испытаний, но тогда результат вычисления этих вероятностей (частот) будет приближенным. Кривая *1* — $P(d)$ для ИНС (ячейки памяти) без повреждений. Кривые *2, 3* — варианты $P(d)$ для ИНС с по-разному случайно выбранными четырьмя ($\sim 44\%$ от их общего числа $N = 9$) входными нейронами, которые погибли со всеми своими межнейронными связями (в (1) соответствующие $w_{ij} = 0$). Кривые *4, 5* — варианты $P(d)$ для ИНС без погибших входных нейронов, но с 25 ($\sim 31\%$ от их общего числа $N^2 = 81$) по-разному случайно выбранными разорванными межнейронными связями.

Из рисунка видно, что для сети без повреждений $P(1) = 0,5$, а для сетей с повреждениями $P(1) < 0,5$, но тем не менее $P(1) > 0$. То есть свободное (без подсказки) вспоминание любой из описанных сетей запомненной в ней информации осуществляется с вероятностью, которая меньше единицы, и поэтому даже при самых благоприятных условиях такого вспоминания (сеть без повреждений) его исход не обязательно положительный. В то же время наличие повреждений обученной сети не исключает возможности безошибочного извлечения запомненной в ней информации, а только делает эту возможность менее вероятной. Так, в частности, проявляется в предлагаемой модели существенно статистический характер процесса извлечения информации из памяти.

Из рисунка также следует, что для неповрежденной сети (кривая *1*) и для сетей с повреждениями (кривые *2–5*) вероятности $P(0)$ узнавания запомненной информации одинаковы и, более того, $P(0) = 1$. При этом вероятности свободного вспоминания $P(1)$ и вспоминания с подсказкой $P(d)$, $0 < d < 1$, для сетей с повреждениями могут быть существенно меньше, чем для неповрежденной сети. В то же время по результатам систематических экспериментальных исследований установлено [11], что по сравнению с нормальными контрольными испытуемыми у пациентов с частичным повреждением фронтальной доли мозга в наибольшей степени ослабевает способность к свободному вспоминанию стимулов и в наименьшей — способность их узнавания. Эта особенность [11] экспериментальных данных, полученных при исследовании памяти здоровых людей и больных с частичным повреждением фронтальных долей мозга, полностью соответствует указанным выше свойствам значений $P(0)$ и $P(1)$ рассматриваемых сетей без повреждений и с повреждениями. Следовательно, такие сети можно использовать для получения количественных результатов при моделировании свойств памяти здорового и частично поврежденного мозга, например, в связи с травмой, болезнью и, возможно, возрастом (предварительные результаты основанного на таком подходе модельного описания свойств удаленной памяти пациентов с частичным повреждением фронтальных долей мозга приведены в [13]).

Описанные ИНС с эталонными векторами, пример которых показан на рисунке (см. [8]), являются также основным элементом компьютерной модели мозга человека, распознающего простые зрительные образы в условиях статистической неопределенности (первое сообщение в [14]).

Предложенный метод компьютерного исследования характеристик ИНС как алгоритмов распознавания (пример результатов для двухслойных сетей показан на рисунке)

можно использовать для выполнения аналогичных исследований элементов памяти любой природы, в частности для исследования сложных ИНС со скрытыми слоями и разным числом нейронов во входном и выходном слое.

В заключение выражаю благодарность академику Н.М.Амосову за внимание к полученным результатам.

Литература

1. Амосов Н.М. — Алгоритмы разума. Киев: Наукова думка, 1979.
2. Кохонен Т. — Ассоциативная память. М.: Мир, 1980.
3. Hopfield J.J. — In: Proc. Nat. Acad. Sci. USA, 1982, v.79, p.2554.
4. Фролов А.А., Муравьев И.П. — Информационные характеристики нейронных сетей. М.: Наука, 1988.
5. Леман Е.Л. — Проверка статистических гипотез. М.: Наука, 1964.
6. Лурия А.Р. — Нейропсихология памяти. М.: Педагогика, 1974.
7. Гопыч П.М., Сорокин В.И., Сотников В.В. — ПТЭ, 1992, №3, с.95; Instr. Exper. Techn., 1992, v.35, No.3, p.446.
8. Гопыч П.М. — ПТЭ, 1998, №3, с.52; Instr. Exper. Techn., 1998, v.41, No.3, p.341.
9. Кисель И.В., Нескоромный В.Н., Ососков Г.А. — ЭЧАЯ, 1991, т.24, с.1551.
10. Hertz J., Krogh A., Palmer R.G. — Introduction to the Theory of Neural Computation. Redwood City, CA. Addison-Wesley, 1991.
11. Wheeler M.A., Stuss D.T., Tulving E. — In: Journ. of the Int. Neuropsych. Soc., 1995, v.1, p.525.
12. Гопыч П.М. — ЭЧАЯ, 1993, т.24, с.1596; Phys. Part. Nucl., 1993, v.24, p.677.
13. Gopych P.M., Gopych I.P. — In: School of Fund. Med. Journ., Kharkov, 1997, v.3, No.2, p.73.
14. Gopych P.M. — In: School of Fund. Med. Journ., Kharkov, 1996, v.2, No.1, p.91.

Рукопись поступила 21 сентября 1999 года.